Mon. Not. R. Astron. Soc. **000**, 000–000 (2010) Printed 21 November 2009 (MN LATEX style file v2.2)

Galaxy evolution from strong lensing statistics: the differential evolution of the velocity dispersion function in concord with the ΛCDM paradigm

Kyu-Hyun Chae⋆
Sejong University, Department of Astronomy and Space Science, 98 Gunja-dong, Gwangjin-Gu, Seoul 143-747, Republic of Korea

Accepted ..... Received .....; in original form .....

ABSTRACT

We study galaxy evolution from $z = 1$ to $z = 0$ as a function of velocity dispersion σ for galaxies with $\sigma \gtrsim 95\,\mathrm{km\ s^{-1}}$ based on the measured and Monte Carlo realised local velocity dispersion functions (VDFs) of galaxies and the revised statistical properties of 30 strongly-lensed sources from the Cosmic Lens All-Sky Survey (CLASS), the PMN-NVSS Extragalactic Lens Survey (PANELS) and the Hubble Space Telescope Snapshot survey. We assume that the total (luminous plus dark) mass profile of a galaxy is isothermal in the optical region for $0 \leqslant z \leqslant 1$ as suggested by mass modelling of lensing galaxies. This study is the first to investigate the evolution of the VDF shape as well as the overall number density. It is also the first to study the evolution of the total and the late-type VDFs in addition to the early-type VDF. For the evolutionary behaviours of the VDFs we find that: (1) the number density of massive (mostly early-type) galaxies with $\sigma \gtrsim 200\,\mathrm{km\ s^{-1}}$ evolves differentially in the way that the number density evolution is greater at a higher velocity dispersion; (2) the number density of intermediate and low mass early-type galaxies ($95\,\mathrm{km\ s^{-1}} \lesssim \sigma \lesssim 200\,\mathrm{km\ s^{-1}}$) is nearly constant; (3) the late-type VDF transformed from the Monte Carlo realised circular velocity function is consistent with no evolution in its shape or integrated number density consistent with galaxy survey results. These evolutionary behaviours of the VDFs are strikingly similar to those of the dark halo mass function (DMF) from N-body simulations and the stellar mass function (SMF) predicted by recent semi-analytic models of galaxy formation under the current ΛCDM hierarchical structure formation paradigm. Interestingly, the VDF evolutions appear to be qualitatively different from "stellar mass-downsizing" evolutions obtained by many galaxy surveys. The coevolution of the DMF, the VDF and the SMF is investigated in quantitative detail based on up-to-date theoretical and observational results in a following paper. We consider several possible systematic errors for the lensing analysis and find that they are not likely to alter the conclusions.

Key words: gravitational lensing – galaxies: formation – galaxies: evolution – galaxies: haloes – galaxies: statistcs – galaxies: kinematics and dynamics

1 INTRODUCTION

The observationally-derived statistical properties of galaxies provide key constraints on models of galaxy formation and evolution. The statistical properties of galaxies include the luminosity functions (LFs), the stellar mass functions (SMFs) and the velocity functions (VFs). In the current Lambda cold dark matter (ΛCDM) hierarchical structure formation picture CDM haloes are formed due to gravitational instabilities and evolve hierarchically through merging (e.g. White & Rees 1978; Lacey & Cole 1993). Baryons settle in the dark matter halo potential wells and undergo dissipational radiative processes including star formations and evolutions, supernovae explosions, AGN activities and their feedback, resulting in visible galaxies (in the central parts of the haloes). Visible galaxies may further merge (and become morphologically transformed) resulting in evolutions of galaxy populations. The various statistical functions of galaxies are the end results of complex processes involving gravitational physics, baryonic physics and merging.

⋆ chae@sejong.ac.kr

The LFs of galaxies have traditionally been measured most extensively and reliably (e.g. Cole et al. 2001; Kochanek et al. 2001; Norberg et al. 2002; Blanton et al. 2003; Croton et al. 2005) and consequently have provided vital constraints on models of galaxy formation and evolution. More recently, the SMFs have been the focus of many observational studies (e.g. Cole et al. 2001; Bell et al. 2003; Drory et al. 2004; Borch et al. 2006; Bundy et al. 2006; Cimatti et al. 2006; Fontana et al. 2006; Pozzetti et al. 2007; Conselice et al. 2007; Scarlata et al. 2007; Marchesini et al. 2009) because they can provide more robust tests of the underlying ΛCDM theory. Recent semi-analytic models of galaxy formation and evolution (e.g. Croton et al. 2006; Bower et al. 2006; Kitzbichler & White 2007; Stringer et al. 2009) appear to match the observed local LFs/SMFs owing in large part to the suitable incorporation of baryonic physics such as AGN feedback.

However, the evolutions of the LFs/SMFs from a high redshift Universe are not understood as well. On the observational side, deep surveys of galaxies have been used to derive the evolutions for the type-specific populations as well as the total population, particular attention paid to photometrically red galaxies or morphologically early-type galaxies which occupy the most massive part of the galaxy population. Various existing observational results on the number density evolution are at variance. Many galaxy survey results (e.g. Cimatti et al. 2006; Bundy et al. 2006; Fontana et al. 2006; Pozzetti et al. 2007; Conselice et al. 2007; Scarlata et al. 2007; Brown et al. 2007; Cool et al. 2008; Marchesini et al. 2009) suggest little evolution of massive (super-L^*) early-type galaxies often accompanying "mass-downsizing" behaviour in which more massive galaxies are to be in place at an earlier time so that the number density of most massive early-type galaxies evolves least while the number density of typical $\sim L^*$ galaxies may evolve significantly over cosmic time. On the other hand, there are also galaxy survey results that do not particularly support mass-downsizing evolutions (e.g. Bell et al. 2004; Ilbert et al. 2006; Faber et al. 2007; Lotz et al. 2008; Ilbert et al. 2009). On the theoretical side, semi-analytic model predictions on the LF/SMF evolutions scatter (e.g. Bower et al. 2006; Menci et al. 2006; Monaco et al. 2006; de Lucia et al. 2006; Kitzbichler & White 2007; Almeida et al. 2008; Cattaneo et al. 2008; Stringer et al. 2009; Fontanot et al. 2009) and are not in good agreement with existing observational constraints on the evolutions of the SMFs, particularly for the type-specific galaxy populations. Semi-analytic models do not predict mass-downsizing evolutions of the SMF and according to more recent studies the mismatch between model predictions and observed SMFs is more severe for less massive galaxies with $M_{\rm stars} \lesssim 10^{11}{\rm M}_\odot$ (e.g. Cattaneo et al. 2008; Stringer et al. 2009; Fontanot et al. 2009).

Given the varying results on galaxy evolutions both observationally and theoretically, it would be of great value to constrain galaxy evolutions through other independent methods based on different data sets. The statistical analysis of strong lensing galaxies in conjunction with well-determined local velocity dispersion functions (VDFs) of galaxies provides such an independent method. The VDFs represent the statistical properties of the dynamics of galaxies that have been modified by baryonic physics from the CDM haloes. The velocities of particles and stars are boosted and the density profiles become steeper. These dynamical features can be seen by comparing the dynamical properties of N-body simulated haloes and the observationally-derived kinematical and dynamical properties of visible galaxies. N-body simulations show that pure CDM haloes follow NFW (or NFW-like) density profiles (e.g. Navarro et al. 1997; Moore et al. 1999; Jing & Suto 2002; Navarro et al. 2004) and hence rising velocity profiles in the inner parts whereas the kinematical and dynamical properties of galaxies, derived from such methods as stellar dynamics (e.g. Rix et al. 1997; Cappellari et al. 2006), rotation curves (e.g. Rubin et al. 1985; Persic et al. 1996; Salucci et al. 2007), gravitational lensing (e.g. Rusin & Kochanek 2005; Koopmans et al. 2006; Gavazzi et al. 2007), show that baryon settled galaxies follow isothermal (or isothermal-like) density profiles implying that velocities are boosted and mass distributions become more concentrated in the inner regions. An important observable quantity that characterises the dynamical state of the galaxy is the line-of-sight velocity dispersion σ especially for rotation-free early-type galaxies. For late-type galaxies, rotations are important in the disk. Nevertheless, the bulge and the surrounding halo of the late-type galaxy may be regarded as an ellipsoidal system that is similar to early-type galaxies. Furthermore, given that most late-type systems are isothermal(-like) as inferred from nearly flat rotation curves, we may relate the circular rotation speed in the disk v_c to the velocity dispersion in the inner halo via $v_c = \sqrt{2}\sigma$.

All three statistical functions (i.e. LF, SMF, and VDF) are the consequences of baryonic physics from pure CDM haloes. However, unlike the other functions the VDF has only to do with the dynamical effects of baryonic physics separated from many other complex effects involving radiative processes. Furthermore, given that galaxy mass profiles are likely to be isothermal(-like) up to significant fractions of the dark halo virial radii as stressed above, we expect a good correlation between the central velocity dispersion and the halo virial mass. Hence the velocity dispersion function (VDF) will be another independent and powerful constraint on galaxy formation and evolution. One advantage of the VDF as a cosmological probe is that it can test the underlying ΛCDM structure formation theory more robustly because it is linked more intimately to the theoretical halo mass function.

In this paper we use a range of local VDFs. The local VDFs include not only the SDSS VDF of early-type galaxies measured by Choi et al. (2007) but also the type-specific and total VDFs obtained through a Monte Carlo method based on the galaxy LFs from the SDSS and intrinsic correlations between luminosity and velocity dispersion or circular rotation speed. We then constrain the evolutions of the VDFs through the statistical analysis of galactic-scale strong gravitational lensing. Strong lensing statistics is a powerful means to constrain the evolution of the VDF because strong lensing probability is proportional to comoving number density times σ^4 (the image separation is proportional to σ^2) and lensing galaxies are distributed over a range of redshifts (up to $z \gtrsim 1$) and virtually over all area of sky. The latter property is particularly important since it means that unlike deep galaxy surveys strong lensing data are free from cosmic

variance. For strong lensing statistics we use a total of 30 lenses from the radio-selected Cosmic Lens All-Sky Survey (CLASS; Myers et al. 2003; Browne et al. 2003) and PMN-NVSS Extragalactic Lens Survey (PANELS; Winn et al. 2001) and the optically-selected Hubble Space Telescope Snapshot survey (Maoz et al. 1993), as these surveys have well-defined selection functions and cover about the same image separation range (i.e., $\gtrsim 0''.3$) and similar redshift ranges for source quasars.[1] However, only the CLASS statistical sample of 13 lenses (Browne et al. 2003; Chae 2003) and the Snapshot sample of 4 lenses are used for the statistics of absolute lensing while the rest of lenses are used only for the distributions of image separations (and lens redshifts if available).

This paper is organised as follows. In §2 we derive through a Monte Carlo method the local VDFs for both the type-specific galaxy populations and the total population. In §3 we describe the strong lensing data and the theoretical model for statistical analysis of strong lensing. In §4 we constrain (non-evolving) intermediate redshift VDFs using strong lensing data and then compare the intermediate redshift VDFs with local VDFs. This simple analysis captures the trends of the evolutions. Next we study in detail the evolution of the VDF through a parametric approach (§5). The results that come out are striking. The number density evolution as a function of σ is differential: the number density of galaxies of typical velocity dispersion and lower evolves little since $z = 1$ but that of larger velocity dispersion evolves significantly showing "velocity upsizing (hierarchical)" behaviour of galaxy evolution. In the discussion section we first consider possible systematic errors (§6.1) and then compare with previous results of strong lensing on galaxy evolutions (§6.2) and the evolutionary behaviours of the DMF and the SMF from the literature (§6.3). A comprehensive analysis of the coevolution of the DMF, the VDF and the SMF is carried out in a companion paper (Chae 2010). We give the conclusions in §7. Throughout we assume a ΛCDM cosmology with $(\Omega_{\rm m0}, \Omega_{\Lambda 0}) = (0.25, 0.75)$ and $H_0 = 100h\,{\rm km\ s^{-1}\ Mpc^{-1}}$ consistent with the WMAP 5 year data (Dunkley et al. 2009). When parameter h does not appear explicitly, $h = 0.7$ is assumed.

2 VELOCITY DISPERSION FUNCTIONS OF GALAXIES AT $Z \approx 0$

2.1 Statistical functions of galaxies

The Schechter luminosity function (LF) $\phi_{\rm L}$, the differential comoving number density as a function of luminosity, is given by

$$dn = \phi_{\rm L}(L)dL = \phi_{\rm L}^* \left(\frac{L}{L^*}\right)^{\alpha_{\rm L}} \exp\left(-\frac{L}{L^*}\right)\frac{dL}{L^*}. \quad (1)$$

It has been measured extensively at various wavebands and recent observations have produced reliable results at optical (e.g. Norberg et al. 2002; Blanton et al. 2003; Croton et al. 2005) and infrared (e.g. Cole et al. 2001; Kochanek et al. 2001) wavebands owing particularly to large surveys such as the Sloan Digital Sky Survey (SDSS), the Two Degree Field Galaxy Redshift Survey (2dF) and the Two Micron All Sky Survey (2MASS).

Given the observed power-law correlations between luminosity and internal velocities of galaxies such as the Faber-Jackson (Faber & Jackson 1976) relation and the Tully-Fisher (Tully & Fisher 1977) relation, one may expect a modified form of the Schechter function for a velocity function. Indeed, Sheth et al. (2003) find that the distribution of the velocity dispersions of early-type galaxies from the SDSS is well fitted by the VDF ϕ of the form

$$dn = \phi(\sigma)d\sigma = \phi^* \left(\frac{\sigma}{\sigma^*}\right)^{\alpha} \exp\left[-\left(\frac{\sigma}{\sigma^*}\right)^{\beta}\right] \frac{\beta}{\Gamma(\alpha/\beta)}\frac{d\sigma}{\sigma}, \quad (2)$$

or equivalently

$$\phi(V)dV = \phi^* 10^{\alpha(V-V^*)} \exp\left[-10^{\beta(V-V^*)}\right] \frac{\beta \ln 10}{\Gamma(\alpha/\beta)} dV, \quad (3)$$

where V is the logarithmic variable given by

$$V = \log_{10}\sigma. \quad (4)$$

Notice that equation (2) along with equation (1) imply the following correlations:

$$\alpha_{\rm L} = \alpha/\beta - 1 \quad \text{and} \quad \phi_{\rm L}^* = \phi^*/\Gamma(\alpha/\beta), \quad (5)$$

where ϕ^* is the integrated comoving number density of galaxies, and an 'effective' power-law correlation between luminosity (L) and velocity dispersion (σ) of

$$\frac{L}{L^*} = \left(\frac{\sigma}{\sigma^*}\right)^{\beta}. \quad (6)$$

However, directly measured relations of $L = L(\sigma)$ and $\sigma = \sigma(L)$ give different values for the power-law slope β compared with that in equation (6) because the scatter in the correlation acts in different ways for the different fits (Sheth et al. 2003). Furthermore, the value of β varies as a function of luminosity as can be seen in a magnitude-velocity dispersion plane of galaxies [see Fig. 1 or Fig. 4b of Choi et al. (2007)]. This is why it is not reliable to turn a LF of galaxies to a VDF simply using equation (5) and a (mean) Faber-Jackson or Tully-Fisher relation although this was often practised in the past. One must fully take into account the intrinsic scatter in the magnitude-velocity dispersion plane. This is done below.

2.2 VDF of early-type galaxies

Choi et al. (2007) have measured the VDF for local early-type galaxies based on a large sample of galaxies from the SDSS DR5 data set, employing a galaxy classification scheme that closely matches visual classifications (Park & Choi 2005). The early-type VDF measured by Choi et al. (2007) will be referred to as 'E0' VDF and can be found in Table 1. Notice, however, that galaxy number counts start to become incomplete at low velocity dispersions for a given galaxy sample used by Choi et al. (2007) because the sample is not limited by velocity dispersion but by absolute magnitude. Choi et al. (2007) discuss this kind of problem for $\sigma < 150\,{\rm km\ s^{-1}}$ and obtain galaxy counts down to $\sigma \approx 70\,{\rm km\ s^{-1}}$ using a series of samples of different volume and magnitude limits. The measurement of the

[1] SDSS quasar lens search (Inada et al. 2008) is limited to image separation range of $\geqslant 1''$ and source redshift range of $0.6 < z < 2.2$.

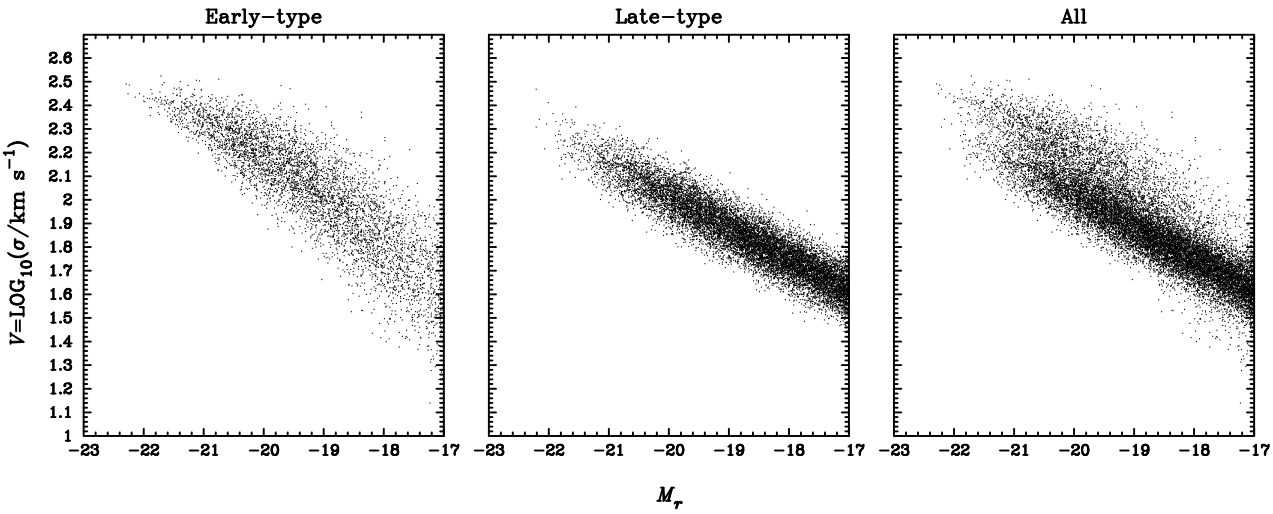

Figure 1. Monte Carlo realised magnitude-velocity dispersion ($M_r - \sigma$) relations. Only 5% of the generated galaxies are shown. The magnitude is the SDSS r-band absolute magnitude. The relation for the early-type population is from the Choi et al. (2007) measured relation while that for the late-type population is inferred from the relation between M_r and the rotational circular speed by Pizagno et al. (2007) assuming a singular isothermal sphere for the total mass distribution of a galaxy. The relation for all galaxies is the combination of the early-type and the late-type relations.

LF is free of this problem at low luminosities down to the absolute magnitude limit of a given sample. Hence galaxy counts are more reliable at low luminosities than low velocity dispersions.

It is therefore desirable to use galaxy counts at low luminosities in deriving the VDF for the full range of velocity dispersions. We use a Monte Carlo method as follows. We generate galaxies within a comoving volume brighter than an absolute magnitude limit according to a measured luminosity function. The next step is to assign a velocity dispersion to each galaxy of a given absolute magnitude. To do this we use the 2-dimensional distribution of galaxies in the absolute magnitude-velocity dispersion ($M - \sigma$) plane. We assume that the most likely value of $V \equiv \log_{10}\sigma$ varies as a function of M_r (absolute magnitude in SDSS r band) according to the Choi et al. (2007) Fig. 4b. We assume that V follows a normal distribution for a given M_r with a varying dispersion of

$$s(M_r) = a(M_r - M_r^*) + s^*, \tag{7}$$

as suggested by the Choi et al. (2007) Fig. 4b. Once all mock galaxies are assigned velocity dispersions, we finally derive the VDF by counting mock galaxies as a function of V.

We consider the SDSS early-type LF by Choi et al. (2007). The Choi et al. (2007) LF is the optimal choice for the following two reasons. First, Choi et al. (2007) classify galaxies using a classification method that matches closely visual classification (Park & Choi 2005). Second, the Choi et al. (2007) LF is based on the same SDSS magnitude system that is used for the magnitude-velocity dispersion relation, so that any error arising from photometric transformations (e.g., from the 2dF magnitude) is avoided. For this LF we derive the early-type VDF using the Monte Carlo method described above adopting $M_r^* - 5\log_{10} h = -20.23$, $s^* = 0.085$ and $a = 0.025$ where s^* and a are chosen so that the simulated $M_r - V$ relation mimics that observed by Choi et al. (2007) with a mean dispersion of ≈ 0.11 for $-22 \lesssim M_r \lesssim -17.5$. The simulation comoving volume is $10^7\ h^{-3}$ Mpc^3 and the faint magnitude limit is $M_r - 5\log_{10} h = -16$. This simulation generates more than 100,000 early-type galaxies. The simulated $M_r - V$ relation for the Choi et al. (2007) early-type LF can be found in Fig. 1. Notice that this simulated plane is very similar to the Choi et al. (2007) Fig. 4b. The derived early-type VDF will be referred to as 'E1' VDF and can be found in Fig. 2 and table 1. Notice that the VDF derived from the Choi et al. (2007) early-type LF closely matches the Choi et al. (2007) measured VDF for $\sigma \gtrsim 150\,\mathrm{km\ s^{-1}}$ but shows significant difference at lower σ. This could mirror the incompleteness in galaxy counts at low velocity dispersions by Choi et al. (2007). Because of this possibility we consider both the Choi et al. (2007) measured VDF and the Monte Carlo realised VDF.

2.3 VDF of late-type galaxies

There does not yet exist any kind of directly measured velocity functions for the late-type population of galaxies. For the late-type population, the internal motions in the optical regions of galaxies are observed as rotations since the (random) motions of dark matter particles are not observed. Unfortunately, it is not an easy observational task to measure the rotation of a galaxy and consequently rotations of galaxies have not been measured for all galaxies in a volume or magnitude limited galaxy sample. However, one may obtain a velocity function for the late-type population from the LF through the Tully-Fisher relation between rotational speed and luminosity that is usually a tighter correlation than the Faber-Jackson relation of the early-type population. For example, Gonzalez et al. (2000), Kochanek & White (2001), Chae (2003) and Sheth et al. (2003) inferred circular velocity functions (CVFs) of late-type galaxies combining various

Table 1. Local statistical functions of galaxies based on SDSS data

Type	ID	α	β	$\alpha_{\rm L}$	ϕ^* (h^3 Mpc^{-3})	$\phi^*_{\rm L}$ (h^3 Mpc^{-3})	$M_r^* - 5\log_{10} h$	σ^* (km s^{-1})	Reference
					Early-type				
VDF	E0	2.32	2.67	-0.13	0.008	0.0073	···	161.	Choi et al. (2007)
LF	···	···	···	-0.527	···	0.0071	-20.23	···	Choi et al. (2007)
VDF	E1	0.85	3.72	-0.77	0.013	0.0033	···	217.	This work
					Late-type				
LF	···	···	···	-0.897	···	0.012	-20.22^a	···	Choi et al. (2007)
VDF	L1	0.69	2.10	-0.67	0.066	0.024	···	91.5	This work
				α'		All ε			
VDF	A0	0.69	2.01	6.61	0.074	0.044	···	100.	This work
VDF	A1	0.69	2.05	7.69	0.078	0.035	···	102.	This work

Notes. [a] An internal extinction of $A_r \approx 0.1$ [extrapolated from Fig. 11 of Pizagno et al. (2007)] is assumed and corrected for the Choi et al. (2007) $b/a > 0.6$ late-type galaxies.

late-type LFs and Tully-Fisher relations. It is also possible to convert the CVF to the VDF via $\sigma = v_{\rm c}/\sqrt{2}$ assuming the singular isothermal sphere model for the total mass distribution of a galaxy.[2] In this work we essentially follow this approach to obtain estimates of the VDF of late-type galaxies. However, we fully take into account the intrinsic scatter in the Tully-Fisher relation using the Monte Carlo method described in §2.2.

The Tully-Fisher relation has been published by numerous authors. The relation is usually expressed as $L/L^* = (v_{\rm c}/v_{\rm c}^*)^\beta$ or its inverse relation $v_{\rm c}/v_{\rm c}^* = (L/L^*)^{1/\beta}$. The slope β ranges from $\approx$ 2.5 - 3.5 in most of the published results in optical and infrared bands (See Pizagno et al. 2007 and references therein). Pizagno et al. (2007) derive the relation $L = L(v_{\rm c})$ and its inverse relation $v_{\rm c} = v_{\rm c}(L)$ for 162 SDSS galaxies in the SDSS g, r, i and z bands. The galaxies used by Pizagno et al. (2007) have apparent minor-to-major axis ratio $b/a \leqslant 0.6$ so that internal extinctions are measured and corrected for reliably. The measurements of the TF relation and its inverse relation give different slopes because of the scatter (as for the FJ relation). Notice that the inverse relation $v_{\rm c}/v_{\rm c}^* = (L/L^*)^{1/\beta}$ is more applicable in deriving a velocity function from the LF because the velocity function is estimated from the LF. For the SDSS r-band Pizagno et al. (2007) find $\log_{10}(v_{\rm c}) = (-0.135\pm0.006)(M_r - M_r^*) + (2.210\pm 0.006)$ with $M_r^* - 5\log_{10} h = -20.332$ and a dispersion of 0.063 ± 0.005. The relation between $V(= \log_{10}\sigma)$ and M_r then follows from $\log_{10}(v_{\rm c}) = V + \log_{10}\sqrt{2}$ for the SIS model of the galaxy.

Using the Monte Carlo method based on the above Pizagno et al. (2007) $M_r - V$ relation the VDF of late-type galaxies is derived for the late-type LF by Choi et al. (2007). As in §2.2 the simulation comoving volume is $10^7\ h^{-3}$ Mpc^3 and the faint magnitude limit is $M_r - 5\log_{10} h = -16$. By this simulation more than 300,000 late-type galaxies are generated. The derived VDF will be referred to as 'L1' VDF and can be found in Fig. 2 and Table 1. Fig. 2 also shows a VDF derived assuming no intrinsic scatter for the Choi et al. (2007) late-type LF to demonstrate the effect of the intrinsic scatter in the Tully-Fisher relation. The simulated $M_r - V$ relation for the Choi et al. (2007) late-type LF can be found in Fig. 1.

[2] Dark matter haloes are, in general, triaxial in shape and have density profiles that deviate from the isothermal profile. Nevertheless, the deviations of shapes and profiles from the SIS may have cancelling effects statistically so that the averaged property of a galaxy might not deviate too much from the SIS.

2.4 VDF of all galaxies

In §2.2 and §2.3 the VDFs are derived for morphologically-typed galaxies. One may well expect that a well-defined VDF exist for the entire population of galaxies. Here we consider this possibility. The total VDF is motivated in several respects. First of all, the total VDF can be compared with theoretical predictions more straightforwardly than type-specific VDFs just as is the total LF because galaxy classifications are not required. Secondly, the evolution of the total VDF is of interest in its own right as it represents the collective evolution of all galaxies including morphological transformations through merging. Thirdly, strong lensing computation is simplified if the total VDF is used because one does not require knowledge of the lensing galaxy type which is not well determined by observations for some systems. Lastly, the observed evolutions of the total LF/SMF may be used for or compared with the evolution of the total VDF.

It is straightforward to derive the total VDF using the Monte Carlo method used above. Early-type and late-type galaxies are separately generated and then combined in the $M_r - V$ plane. For the comoving volume of $10^7\ h^{-3}$ Mpc^3 and the faint magnitude limit of $M_r - 5\log_{10} h = -16$ over 400,000 velocity dispersions of galaxies are used to derive the total VDF. Again we consider the LFs by Choi et al. (2007). We also consider the early-type VDF directly measured by Choi et al. (2007). The derived total VDFs can be found in Fig. 2. The 'A0' VDF corresponds to the combination of the E0 VDF and the L1 VDF while the 'A1' VDF corresponds to that of the E1 and the L1. Notice that the

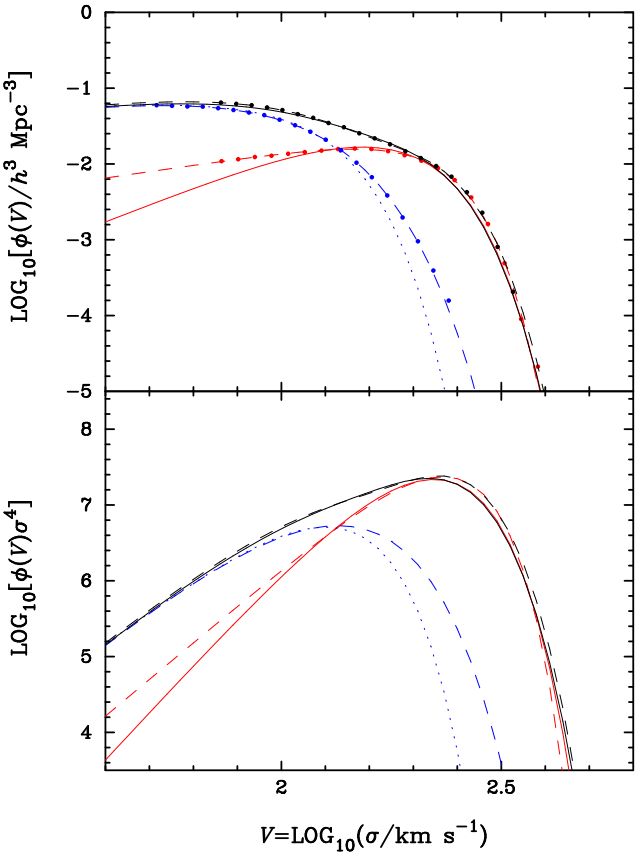

Figure 2. (*Upper panel*) The local velocity dispersion functions of galaxies based on SDSS data (see also Table 1). The red, blue and black curves represent respectively the VDFs for the early-type, the late-type and all populations. The dashed curves are Monte Carlo realised VDFs. The red solid curve is the early-type E0 VDF measured by Choi et al. (2007). The black solid curve is the total VDF resulting from the combination of the E0 VDF and the Monte Carlo realised late-type VDF. The blue dotted curve is the late-type VDF that would be obtained ignoring the intrinsic scatter in the magnitude-velocity relation. (*Lower panel*) The behaviours of $\phi(V)\times\sigma^4$ where $\phi(V)$ is the differential number density of galaxies and σ^4 is proportional to the lensing cross section of each galaxy (assuming the isothermal galaxy profile). These curves show the relative lensing efficiencies of the early-type and the late-type galaxy populations as a function of velocity dispersion.

simulated data points for the total population of galaxies are not fitted well by the VDF of equation (2) in contrast to the morphologically-typed galaxy populations. This might be the true nature of the total VDF. However, it could be due to the errors in the adopted correlations between luminosity and velocity especially at low velocities.[3]

In order to fit successfully the total VDF from the present data we consider the following function that includes a correction term for high velocity dispersions,

$$\phi_{\rm tot}(\sigma)d\sigma = \phi^*\left[(1-\varepsilon)\left(\frac{\sigma}{\sigma^*}\right)^{\alpha}+\varepsilon\frac{\Gamma(\alpha/\beta)}{\Gamma(\alpha'/\beta)}\left(\frac{\sigma}{\sigma^*}\right)^{\alpha'}\right] \times\exp\left[-\left(\frac{\sigma}{\sigma^*}\right)^{\beta}\right]\frac{\beta}{\Gamma(\alpha/\beta)}\frac{d\sigma}{\sigma}, \quad (8)$$

where ϕ^* is the total number density and ε represents the fraction of the number density due to the second (correction) term. Fig. 2 shows that the total VDFs are well fitted by equation (8). For the fitting process there arises a weak degeneracy between parameters α and ε. To break the degeneracy we fix the value of α to that for the late-type VDF since late-type galaxies dominate in the low velocity dispersion limit. The fitted parameters of the total VDFs can be found in Table 1.

3 STRONG LENSING STATISTICS: DATA AND MODEL

3.1 Data

For the purpose of this work we need galactic-scale strong lens samples that satisfy well-defined observational selection criteria. Such statistical lens samples that have been published so far include those from the radio-selected CLASS and PANELS surveys (Myers et al. 2003; Browne et al. 2003; Winn et al. 2001) and the optically-selected HST Snapshot (Maoz et al. 1993) and SDSS Quasar Lens Search (QLS: Inada et al. 2008) surveys. However, the SDSS QLS lens systems are limited to image separations greater than 1 arc second while the other surveys include subarcsecond systems down to $\approx 0''.3$. Moreover, the SDSS QLS lens systems are from relatively low-redshift ($0.6 < z < 2.2$) sources while the other surveys include high-redshift sources. For these reasons we use only the HST Snapshot and the CLASS/PANELS lens samples to study the evolutions of the VDFs. The HST Snapshot data include 4 lens systems out of 506 quasars with $z > 1$. The HST Snapshot lens systems are summarised in Table 2 and the data for the entire sources can be found in Maoz et al. (1993). We use the selection function for the Snapshot survey described by Maoz & Rix (1993) and the source number-magnitude relation described by Kochanek (1996) to calculate magnification biases and cross sections. The CLASS data include 22 lens systems out of 16521 radio sources. However, only a subsample of 8958 sources including 13 lens systems, referred to as the CLASS statistical sample, satisfies well-defined selection criteria (see Chae 2003; Browne et al. 2003) so as to allow reliable calculation of cross sections and magnification biases. We use the CLASS selection function and source properties described by Chae (2003) except that we use the number-flux density relation slightly updated by McKean et al. (2007a). The rest of 9 lens systems from the CLASS and additional 4 lens systems from the PANELS (the southern sky counterpart of the CLASS) can be used for relative lensing probabilities (see Chae 2005). The CLASS and PANELS lens systems can be found in Table 2.

Notice that in Table 2 both the image separation $\Delta\theta$ and twice the average radial separation $\langle 2R_i\rangle$ are given for each lens system. $\Delta\theta$ is the maximum possible separation amongst the image components. This is the value adopted

[3] Here it is interesting to note that the early-type and the late-type populations are well fitted by Schechter luminosity functions both separately and in combination although they are well separated photometrically.

Table 2. Summary of Strongly-lensed Sources. The properties of the strongly lensed systems from the Snapshot optical survey and the CLASS (Browne et al. 2003) and PANELS radio surveys are revised from Kochanek (1996) and Chae (2003, 2005). The first 13 radio sources (B0218+357 through B2319+051) are members of the well-defined CLASS statistical sample of 8958 radio sources (Browne et al. 2003; Chae 2003). The CLASS statistical sample along with the Snapshot sample are used fully for all their observed properties while the rest of the sources are used only for their relative image separation probabilities. Notations are the following: m_B - B magnitude; f_5 - flux density at 5 GHz; z_s - source redshift; z_l - lens redshift; $\Delta\theta$ - the maximum separation between any pair of the images; $\langle 2R_i \rangle$ - twice the average separation of the images from the primary lensing galaxy (or the image centre if the lens is not observed); $N_{\rm im}$ - number of images; E/L - early/late-type galaxy; CL - lensing cluster/group; G2 - secondary (satellite) lensing galaxy. References are the following: 1 - the CASTLES website (http://cfa-www.harvard.edu/castles/); 2 - Chae (2003, 2005); 3 - Kochanek (1996); 4 - Siemiginowska et al. (1998); 5 - York et al. (2005); 6 - Biggs et al. (2003); 7 - Rusin et al. (2001); 8 - Surpi & Blandford (2003); 9 - Cohn et al. (2001); 10 - McKean et al. (2007b); 11 - Chae et al. (2001); 12 - Phillips et al. (2000); 13 - Winn et al. (2003); 14 - Lehár et al. (2000); 15 - King et al. (1997); 16 - More et al. (2008)

Source	Survey	$m_{\rm B}$/ f_5 [mJy]	z_s	z_l	$\Delta\theta$ [$''$]	$\langle 2R_i \rangle$ [$''$]	$N_{\rm im}$	Lens Type	Comments	References
Q0142-100	Snapshot	16.8	2.72	0.49	2.23	2.24	2	E		1, 3
PG1115+080	Snapshot	16.1	1.72	0.31	2.43	2.32	4	E	Group	1, 3
Q1208+1011	Snapshot	17.9	3.80	1.13?	0.48	0.48	2	?		1, 3, 4
H1413+117	Snapshot	17.0	2.56	—	1.10	1.24	4	?(E)[a]		1, 3
B0218+357	CLASS	1480.	0.96	0.68	0.33	0.34	2	L		1, 2
B0445+123	CLASS	50.	—	0.56	1.32	1.35	2	E		1, 2
B0631+519	CLASS	88.	—	0.62	1.16	1.17	2	E		2, 5
B0712+472	CLASS	30.	1.34	0.41	1.27	1.46	4	E	Group	1, 2
B0850+054	CLASS	68.	—	0.59	0.68	0.68	2	L		2, 6
B1152+199	CLASS	76.	1.02	0.44	1.56	1.59	2	2Gs [?(E)[a]+?]	G2 ignored	1, 2
B1359+154	CLASS	66.	3.24	≈ 1	1.67	1.71	6	3Gs (E+?+?)	Group	1, 2, 7
B1422+231	CLASS	548.	3.62	0.34	1.24	1.68	4	E	Group	1, 2
B1608+656	CLASS	88.	1.39	0.64	2.09	2.34	4	2Gs (E+L)	Group	2, 8
B1933+503	CLASS	63.	2.62	0.76	1.16	1.02	4+4+2	E		2, 9
B2045+265	CLASS	55.	?[b]	0.87	1.91	2.34	4	2Gs (E+?)		2, 10
B2114+022	CLASS	224.	—	0.32/0.59	2.56	2.62	2 or 4	2Gs (E+E)	Group	2, 11
B2319+051	CLASS	76.	—	0.62	1.36	1.36	2	E	Group	1, 2
B0128+437	CLASS	—	3.12	1.15	0.55	0.46	4	?		2, 12
J0134−0931	PANELS	—	2.23	0.76	0.68	0.81	5+2	2Gs (L?+L?)		1, 2, 13
B0414+054	CLASS	—	2.64	0.96	2.03	2.40	4	E		1, 2
B0739+366	CLASS	—	—	—	0.53	0.53	2	?		1, 2
B1030+074	CLASS	—	1.54	0.60	1.62	1.63	2	2Gs (E+?)	G2 ignored	1, 2, 14
B1127+385	CLASS	—	—	—	0.71	0.74	2	L		1, 2
B1555+375	CLASS	—	—	—	0.41	0.47	4	?		1, 2
B1600+434	CLASS	—	1.59	0.41	1.38	1.40	2	L	Group	1, 2
J1632−0033	PANELS	—	3.42	1?	1.47	1.47	2	E		1, 2
J1838−3427	PANELS	—	2.78	0.36	0.99	0.99	2	E		1, 2
B1938+666	CLASS	—	$\gtrsim 1.8$	0.88	0.91	0.85	4+2+R	E		1, 2, 15
J2004−1349	PANELS	—	—	—	1.13	1.18	2	L		1, 2
B2108+213	CLASS	—	—	0.37	4.57	4.57	2	2Gs (E+E)	Group	1, 2, 16

[a] Assumed early-type for their large inferred velocity dispersions of $\sigma \approx 270\,{\rm km\ s^{-1}}$ for H1413+117 and $\sigma \approx 230\,{\rm km\ s^{-1}}$ for B1152+199.
[b] Fassnacht et al. (1999) suggests $z_s = 1.28$ based only on a single broad emission line. This value for z_s implies an uncomfortably large SIS velocity dispersion of $\sigma \approx 384\,{\rm km\ s^{-1}}$ for G1. However, Hamana et al. (2005) reports a measured central stellar velocity dispersion of $\sigma = 213 \pm 23\,{\rm km\ s^{-1}}$. An alternative value for z_s would be 4.3 assuming the emission line is a Lyman alpha line. We take the latter value for this work.

in previous studies (e.g. Chae 2003, 2005). $\langle 2R_i \rangle$ is two times the average of the separations of the image components from the primary lensing galaxy position or the image centre if the lensing galaxy position is not known. If the lens were an SIS, the two values would be the same. However, for many systems the two values are somewhat different, $\langle 2R_i \rangle$ usually being somewhat larger than $\Delta\theta$. The systems with relatively large differences tend to be quadruply imaged systems with highly asymmetrical morphologies. The average values for all 30 lens systems are $\Delta\theta = 1''.38$ and $\langle 2R_i \rangle = 1''.45$ respectively while those for 9 lens systems that are only quadruply imaged are $\Delta\theta = 1''.45$ and $\langle 2R_i \rangle = 1''.63$ respectively. If we exclude 6 multiple-lens systems, the average separations for the rest 24 systems are $\Delta\theta = 1''.17$ and $\langle 2R_i \rangle = 1''.21$ respectively. Although the differences between $\Delta\theta$ and $\langle 2R_i \rangle$ are not large, we consider the two possibilities in order to be as precise as possible. The question is then which of the two choices would correspond more accurately to the velocity dispersion of the primary lensing galaxy. Because the velocity dispersion is directly related to the Einstein radius R_E (i.e. the critical radius) via a lens model (see, e.g., Chae 2003), the answer may be found by comparing $\Delta\theta$ and $\langle 2R_i \rangle$

with $2R_E$. The Einstein radius R_E for a lens can only be reliably determined from a detailed modelling of the system. This is particularly true for highly asymmetrical systems with large shears. Congdon & Keeton (2005) model some of highly asymmetrical quadruple lens systems through a lens model with the isothermal radial profile and general angular structures. The highly asymmetrical systems that are analysed by Congdon & Keeton (2005) include B0712+472, B1422+231 and B2045+265. As shown in Table 2, for these systems the values for $\Delta\theta$ and $\langle 2R_i\rangle$ are quite different. If we take the Einstein radii found by Congdon & Keeton (2005) for these systems, then $2R_E$ are between $\Delta\theta$ and $\langle 2R_i\rangle$ but much closer to $\langle 2R_i\rangle$. This means that $\langle 2R_i\rangle$ is probably the better choice for this work. Hence the results from this work are based on $\langle 2R_i\rangle$ rather than $\Delta\theta$.

Another important issue regarding the proper interpretation of the lens data is how to treat the multiple-lens systems. The operational definition for a multiple-lens system to be adopted in this work is a system in which the centres of distinct multiple lensing galaxies are found within the Einstein radius of the lens. For such a multiple-lens system care must be taken in interpreting the image separation. If secondary galaxies are much less massive than the primary galaxy and/or lie well outside the Einstein ring, then secondary galaxies may contribute little to the Einstein mass so that the image separation may well correspond to the velocity dispersion of the primary galaxy up to small errors. Clearly, this appears to be the case at least for B1152+199 and B1030+074. On the other hand, if the lensing galaxies are of comparable mass and/or well within the Einstein radius as in interacting galaxies or a chance alignment (in projection) of galaxies at the same redshift (as in a group) or at different redshifts, then the image separation cannot match well the velocity dispersion of the primary galaxy. This appears to be the case for the majority of the multiple-lens systems. Table 3 summarises the Einstein radii of the lensing galaxies in the multiple-lens systems. Indeed, the difference between the Einstein radius of the total lens potential approximated by $\langle R_i\rangle$ and that of the primary lensing galaxy $R_{\rm E}^{(1)}$ is quite large. This means that taking the face values of $\langle 2R_i\rangle$ of the multiple-lens systems would make a significant error in a statistical analysis of strong lensing. Simply ignoring the image separations of the multiple-lens systems would not be a perfect solution either because the primary galaxies of the multiple-lens systems might be biased compared with 'single' lensing galaxies. The average value of $R_{\rm E}^{(1)}$ for the 6 multiple-lens systems in Table 3 is $0''.79$ while that for the rest of 24 systems is $\approx \langle 2R_i\rangle/2 = 0''.61$. If B2108+213 were excluded assuming that the large separation is assisted by a group/cluster, then the average value of $R_{\rm E}^{(1)}$ would be $0''.60$. However, the measured velocity dispersion of G1 in B2108+213 appears to be consistent with the large separation without any significant contribution from the group/cluster (More et al. 2008) implying that B2108+213 may well be a valid data point. Therefore, for the multiple-lens systems we use $2R_{\rm E}^{(1)}$ instead of $\langle 2R_i\rangle$ in our analyses. In doing so, we treat multiple-lens systems as if they were single-lens systems but with corrected image separations.

3.2 Model

Suppose that there is a population of cosmological sources described by a luminosity function or a number-flux density relation $N_{z_s}(>f_\nu)$ (number of sources with flux density greater than f_ν in a certain comoving volume). Then, for a source with observed redshift z_s and flux density f_ν the probability that it is multiply-imaged (with a certain image multiplicity) by intervening galaxies is, crudely speaking,

$$\begin{aligned}\text{probability} &= \text{distance to the source}\\ &\times \text{number density of galaxies}\\ &\times \text{multiple-imaging cross section}\\ &\times \text{magnification bias}\end{aligned} \tag{9}$$

and can be formulated as follows in the order of the four factors:

$$\begin{aligned}p(z_s,f_\nu) &= \int_0^{z_s} dz \left|\frac{cdt}{dz}\right| \int_{\Delta\theta_{\rm min}}^{\infty} d(\Delta\theta)\\ &\times \int_0^{\infty} d\sigma \phi(\sigma,z) s(\sigma,z) \int_{\mu_{\rm min}}^{\infty} \frac{d\mu}{\mu} \mathcal{P}_\sigma(\Delta\theta,\mu)\\ &\times \left|\frac{dN_{z_s}(>f_\nu/\mu)}{df_\nu}\right| \left|\frac{dN_{z_s}(>f_\nu)}{df_\nu}\right|^{-1},\end{aligned} \tag{10}$$

where t is cosmic time (i.e. proper time of a comoving galaxy), $\phi(\sigma,z)$ is the velocity dispersion function, $s(\sigma,z)$ is the cross section of a galaxy with velocity dispersion σ at redshift z, and $\Delta\theta_{\rm min}$ and $\mu_{\rm min}$ are respectively the minimum allowed values of the separation and the magnification. In equation (10), $\mathcal{P}_\sigma(\Delta\theta,\mu)$ is the probability density distribution of image separation ($\Delta\theta$) and magnification (μ) within the multiple-imaging region for a galaxy of velocity dispersion σ. $\mathcal{P}_\sigma(\Delta\theta,\mu)$ depends on the lens model. For the simple case of the singular isothermal sphere (SIS) it is given by

$$\mathcal{P}_\sigma(\Delta\theta,\mu) = \delta(\Delta\theta - \Delta\theta_{\rm SIS}) \frac{2\mu_{\rm min}^2}{\mu^3} \tag{11}$$

with

$$\Delta\theta_{\rm SIS} = 8\pi \frac{r_A(z,z_s)}{r_A(0,z_s)} \left(\frac{\sigma}{c}\right)^2, \tag{12}$$

where c is the speed of light in vacuum and $r_A(z_1,z_2)$ is the angular-diameter distance between redshifts z_1 and z_2 in units of the Hubble radius.

We use the singular isothermal ellipsoid (SIE) lens model described by Chae (2003) to calculate lensing probabilities for a population of galaxies given by a VDF (equation 2). We assume a mean projected mass density axis ratio of 0.7 ignoring the scatter. The expressions for absolute lensing probabilities, i.e. those including magnification biases, can be found in Chae (2003) while relative probabilities of image separations can be found in Chae (2005). The total likelihood for lensing due to a certain population of galaxies is given by

$$\ln \mathcal{L}_{\rm tot} = \ln \mathcal{L}_{\rm opt} + \ln \mathcal{L}_{\rm rad}, \tag{13}$$

where $\mathcal{L}_{\rm opt}$ is the likelihood due to optically selected sources given by

$$\ln \mathcal{L}_{\rm opt} = \sum_{k=1}^{N_{\rm U}^{\rm (opt)}} \ln[1-p^{\rm (opt)}(k)] + \sum_{l=1}^{N_{\rm L}^{\rm (opt)}} \ln \delta p^{\rm (opt)}(l), \tag{14}$$

Table 3. Multiple-lens systems

System	G1's ER $R_{\rm E}^{(1)}$	$2R_{\rm E}^{(1)}$	G2's ER $R_{\rm E}^{(2)}$	G3's ER $R_{\rm E}^{(3)}$	$\langle R_i\rangle - R_{\rm E}^{(1)}$	Comments	Reference
B1152+199	≈ 0.8	···	···	···	≈ 0	G2 ignored	
B1359+154	0.36	0.72	0.29	0.29	0.50		Rusin et al. (2001)
B1608+656	0.53	1.06	0.29	···	0.64		Koopmans et al. (2003)
B2045+265	1.06	2.12	0.09	···	0.11		McKean et al. (2007b)
B2114+022	0.89	1.78	0.46	···	0.42	two-plane lensing	Chae et al. (2001)
J0134−0931	0.17	0.34	0.17	···	0.24		Keeton & Winn (2003)
B1030+074	≈ 0.8	···	···	···	≈ 0	G2 ignored	
B2108+213	1.74	3.48	0.51	···	0.55	cluster/group ignored	More et al. (2008)

Notes: $R_{\rm E}^{(n)}$ – n-th lensing galaxy's (Gn's) Einstein radius (ER); $\langle R_i\rangle$ – the average separation of the images from the primary galaxy (G1). All the values are given in arcseconds.

and $\mathcal{L}_{\rm rad}$ is the likelihood due to radio-selected sources given by

$$\ln\mathcal{L}_{\rm rad} = \left(\sum_{k=1}^{N_{\rm U}^{(\rm rad)}} \ln[1-p^{(\rm rad)}(k)] + \sum_{l=1}^{N_{\rm L}^{(\rm rad)}} \ln\delta p^{(\rm rad)}(l)\right) + \left(\sum_{j=1}^{N_{\rm IS}^{(\rm rad)}} \ln\delta p_{\rm IS}^{(\rm rad)}(j)\right). \quad (15)$$

Then a "χ^2" is defined by

$$\chi^2 = -2\ln\mathcal{L}_{\rm tot}. \quad (16)$$

Here $p(k)$ is the integrated multiple-imaging probability, $\delta p(l)$ is the differential lensing probability of the specific separation, lens and source redshifts, and $\delta p_{\rm IS}(j)$ is the relative image separation probability.

For equation (14) the Snapshot data are used. The lensed systems are the 4 systems of the first part in table 2 and $N_{\rm U}^{(\rm opt)} = 502$. For equation (15) the CLASS and PANELS data are used. For the first parenthesis in equation (15) the lensed systems are the 13 systems of the 2nd part of Table 2 and $N_{\rm U}^{(\rm rad)} = 8945$. For the second parenthesis in equation (15) the lensed systems are the 13 systems of the 3rd part of Table 2.

We calculate lensing statistics for three kinds of galaxy population, i.e. the early-type, the late-type and the total population. For the population of a certain morphological-type we must include only the lensed systems of the same morphological-type lensing galaxies. However, for several lensed systems the lensing galaxy types have not yet been determined by observations nor could be judged otherwise. These systems include Q1208+1011, B0128+437, B0739+366 and B1555+375. These systems all have relatively small image separations. Each of these systems may well be either early-type or late-type. Hence we include these systems for the statistics of both the early-type and the late-type populations but with their contributions to the χ^2 multiplied by a penalisation factor of 0.5.

4 COMPARING THE LOCAL VDFS WITH INTERMEDIATE REDSHIFT ($0.3 \lesssim Z \lesssim 1$) VDFS

For the source redshift distributions of the CLASS and the Snapshot the likely redshift of the lensing galaxy lies in $0.3 \lesssim z \lesssim 1$ (see Table 2). Because of this, if we constrain a non-evolving VDF using the lens data the constrained VDF would correspond to an averaged VDF over the redshift range or a VDF at $z \sim 0.65$ assuming the evolution is smooth in z. Comparing the constrained VDF of a certain galaxy population with the corresponding local VDF may then reveal the essential features of the evolution of the VDF.

We constrain the VDF of the form given by equation (2) for both the type-specific VDFs and the total VDF. The local total VDF is well-fitted by the six-parameter function of equation (8) rather than the function of equation (2) (see §2.4). However, the number statistics of the strong lens sample is not strong enough to warrant the six-parameter function. When all four parameters of the VDF (equation 2) are allowed to vary, the confidence regions in the parameter space are broad because of parameter degeneracies. However, the VDF itself is constrained well within plausible ranges of the parameters. Hence we may fix the low-velocity end slope α to the local value to break the parameter degeneracy without significantly altering the possible range of the VDF.

Fig. 3 shows the 68% and 95% confidence limits (CLs) of the constrained VDF for the total and the type-specific galaxy populations. In Fig. 3 the local VDFs are overplotted and compared with the constrained VDFs. We notice the following trends for the evolutions of the VDFs. First, the number density of highest velocity dispersion galaxies appears to evolve most as can be seen from both the total VDF and the early-type VDF. Second, the lower velocity dispersion part of the early-type VDF does not show any signature of evolution. Finally, the late-type VDF evolves little overall.

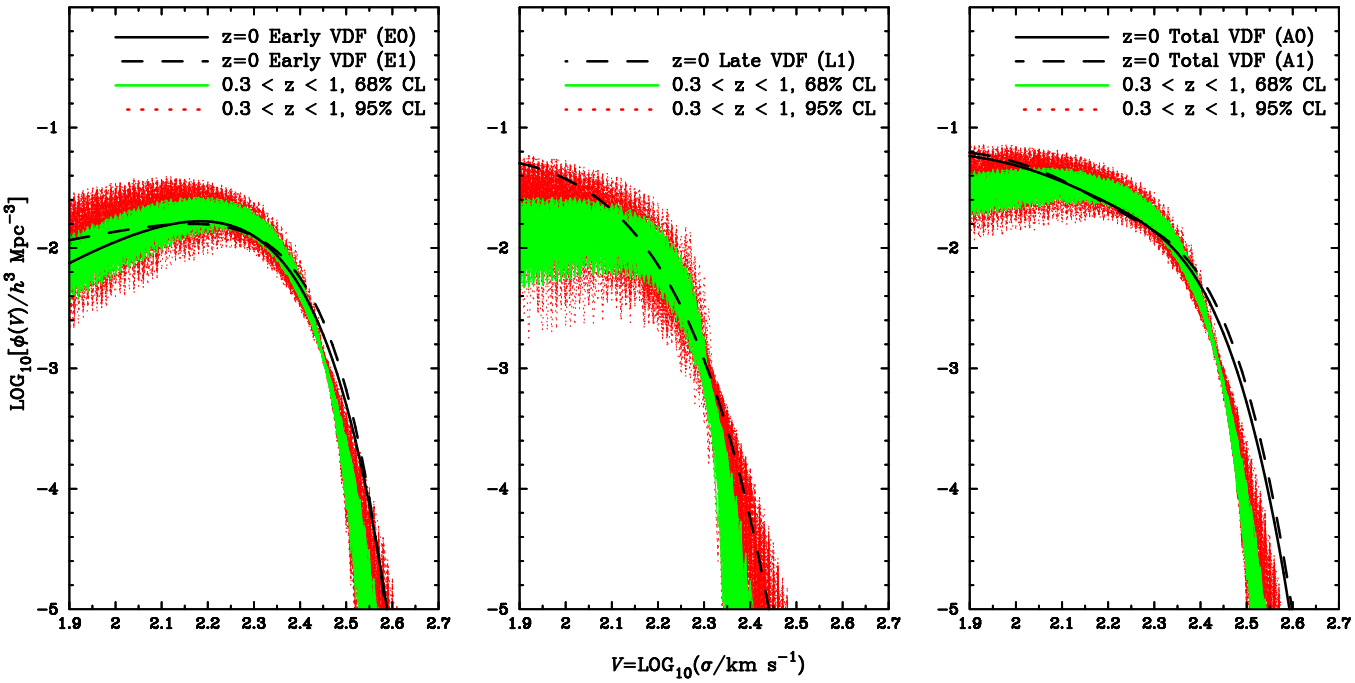

Figure 3. The strong lensing constrained intermediate-redshift ($0.3 \lesssim z \lesssim 1$) VDFs are compared with the local VDFs (Fig. 2 and table 1). These simple comparisons reveal the trends of the evolutions without detailed modelling. The green and red regions are respectively the 68% and the 95% confidence limits.

5 CONSTRAINTS ON THE EVOLUTIONS OF THE VELOCITY DISPERSION FUNCTIONS: PARAMETRIC MODELLING

We study the evolution of the VDF through a parametric approach. We parametrise the evolution of the number density and the velocity dispersion as

$$\phi^*(z) = \phi_0^* 10^{Pz}; \quad \sigma^*(z) = \sigma_0^* 10^{(Q/4)z}, \tag{17}$$

and the evolution of the shape of the VDF as

$$\alpha(z) = \alpha_0 \left(1 + k_\alpha \frac{z}{1+z}\right); \quad \beta(z) = \beta_0 \left(1 + k_\beta \frac{z}{1+z}\right). \tag{18}$$

Here z is the cosmological redshift and $z/(1+z) = 1-(a/a_0)$ (where a and a_0 are the cosmological scale factors at redshift z and zero respectively). Parameters P and Q in equation (17) are parametrised such that they have the same sensitivity to the strong lensing optical depth (the absolute lensing probability). The positivity of α and β in equation (18) requires that $k_\alpha > -1$ and $k_\beta > -1$. Notice that parameters Q, k_α and k_β have sensitivities to the image separation distributions as well as the lensing optical depth while parameter P has sensitivity only to the lensing optical depth.

The present lens sample is limited to the image separation $\Delta\theta \gtrsim 0''.3$. Consequently, the data cannot constrain the shape of the VDF for $\sigma \lesssim 95\,\mathrm{km\ s^{-1}}$.[4] Hence the constraints from this study are valid only for $\sigma \gtrsim 95\,\mathrm{km\ s^{-1}}$ and outside this range the results must be regarded as extrapolations. Because of this limitation of the lens data and the small number statistics parameter k_α is ill-constrained by the data. Moreover, for a given shape of the VDF there are parameter degeneracies as pointed out in §4. Hence it is necessary to impose a constraint on the parameters. We may consider $k_\alpha = 0$ or $k_\alpha = k_\beta$ as a default choice. The former choice corresponds to a constant shape for the low velocity end slope while the latter corresponds to a constant faint-end slope since $\alpha_\mathrm{L} = \alpha(z)/\beta(z) - 1$ (equation 5). In practise these two choices make little difference for the present data. We adopt the latter constraint because the intermediate-redshift VDFs constrained in §4 appear to be steeper both at the low velocity and the high velocity ends.

5.1 Early-type galaxies

Fig. 4 shows the 68% and 95% CLs in the P-Q plane for two local early-type VDFs. The fitted parameter values can be found in Table 4. The early-type VDFs (both the Choi et al. (2007) measured E0 VDF and the Monte Carlo generated E1 VDF) evolve little overall. The overall little evolution of the early-type VDF is consistent with previous constraints from strong lensing statistics (e.g. Chae & Mao 2003; Ofek et al. 2003).

However, more detailed nature of the evolution as a function of velocity dispersion can be found in Fig. 5 in which the local VDFs are compared with the corresponding projected VDFs at $z = 1$. The main features of Fig. 5 may

[4] For a lens redshift of 0.6 and a source redshift of 2. $\Delta\theta = 0''.3$ corresponds to $\sigma \approx 95\,\mathrm{km\ s^{-1}}$ for the assumed cosmology.

Table 4. Evolution parameters for the velocity dispersion functions

VDF	P	Q	k_β
	Early-type		
E0	$+0.02^{+0.38}_{-0.32}$	$-0.08^{+0.33}_{-0.48}$	$+0.12^{+0.67}_{-0.57}$
E1	$-0.15^{+0.46}_{-0.34}$	$-0.01^{+0.21}_{-0.38}$	$+0.65^{+1.05}_{-0.97}$
	Late-type		
L1	$-0.56^{+0.74}_{-0.66}$	$+0.40^{+0.56}_{-0.84}$	$+0.34^{+0.93}_{-0.81}$
	All		
A0	$+0.73^{+0.23}_{-0.28}$	$-1.87^{+0.86}_{-0.63}$	$-0.71^{+0.30}_{-0.16}$
A1	$+0.81^{+0.21}_{-0.23}$	$-2.18^{+0.79}_{-0.56}$	$-0.77^{+0.25}_{-0.13}$

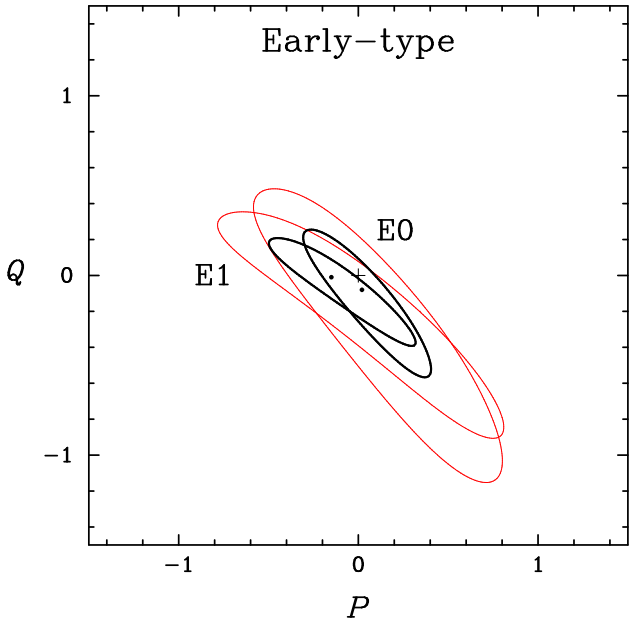

Figure 4. The 68% and the 95% confidence limits in the evolutionary parameters of the early-type velocity dispersion function. The integrated number density evolves as 10^{Pz} while the velocity dispersion parameter $\sigma^* \propto 10^{Qz/4}$. The parameter for the evolution of the shape is not shown here but can be found in table 4.

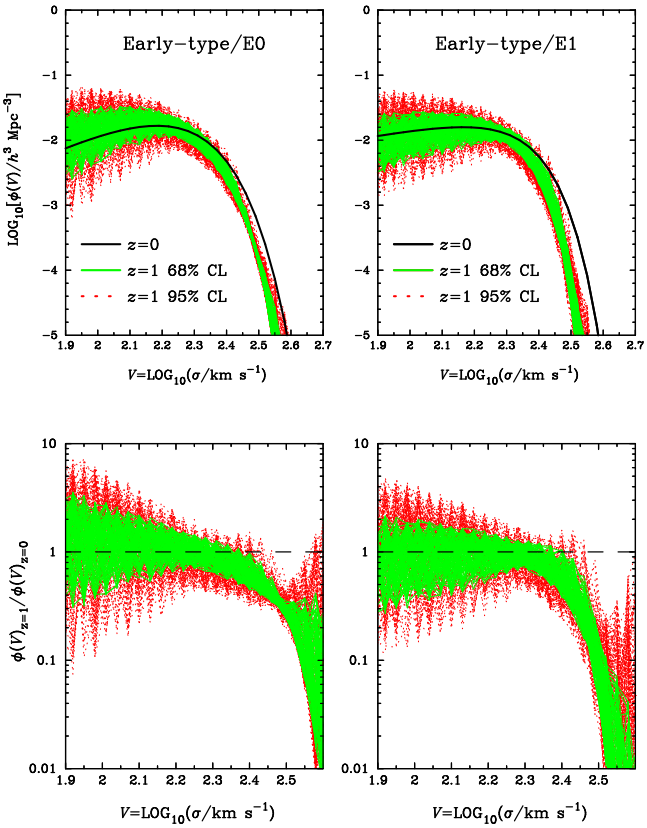

Figure 5. The early-type VDFs at $z = 1$ are compared with the local counterparts. The $z = 1$ VDFs are the functions projected using the constrained evolution parameters (table 4). The green and red regions show the 68% and 95% confidence limits due to the uncertainties in the constrained parameters. These figures clearly show the differential number density evolution for early-type galaxies of high velocity dispersion in which the evolution is greater at a higher velocity dispersion.

be summarised as follows. First, the number densities of early-type galaxies of large velocity dispersions ($\sigma \gtrsim 230 - 250\,\mathrm{km\ s^{-1}}$) have not only changed significantly from $z = 1$ to $z = 0$ but by an increasingly larger factor for a larger velocity dispersion. The dependence of the number density evolution on velocity dispersion appears to be real because a constant shape is clearly disfavoured by data. In particular, the number density of the largest velocity dispersion galaxies ($\sigma \gtrsim 300\,\mathrm{km\ s^{-1}}$) has increased by a large factor ($\gtrsim 3$) since $z = 1$. Second, for early-type galaxies of typical velocity dispersions and lower ($\sigma \lesssim 230 - 250\,\mathrm{km\ s^{-1}}$) there is no statistically significant change in number density from $z = 1$ to $z = 0$. This explains why lens statistics gives the "right" cosmology assuming no evolution in the number density and the shape (see §6.2).

Finally, we must bear in mind that the above results for the early-type population suffer from systematic errors arising from the lack of the knowledge of the lensing galaxy morphological type for several lens systems (see §3). The results for the late-type population shown below are prone to the same problem. However, the results for the evolution of the total VDF (§4.3) are free from the problem.

5.2 Late-type galaxies

The evolutionary behaviours of the late-type VDF can be found in Figs. 6 & 7. Overall, the late-type VDF is consistent with no evolution at the 68% confidence level. Furthermore, in contrast to the early-type VDF there is no statistically significant differential evolution for the late-type VDF. In particular, the number density of the most massive late-type galaxies does not change significantly between $z = 1$ and $z = 0$.

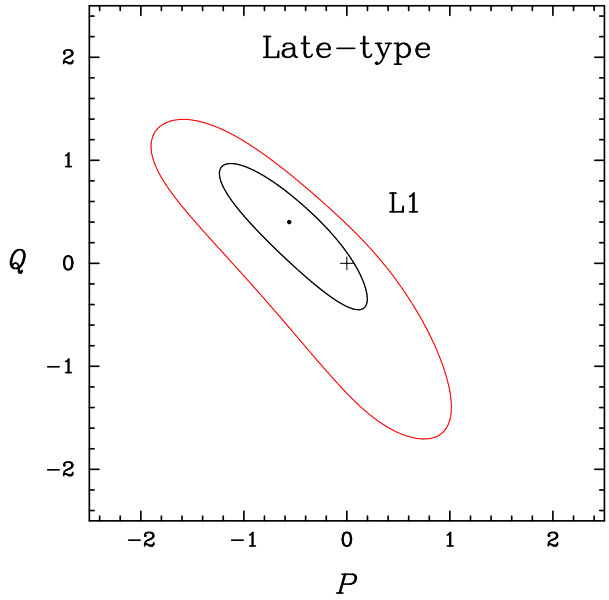

Figure 6. The same as Fig. 4 but for the late-type population of galaxies.

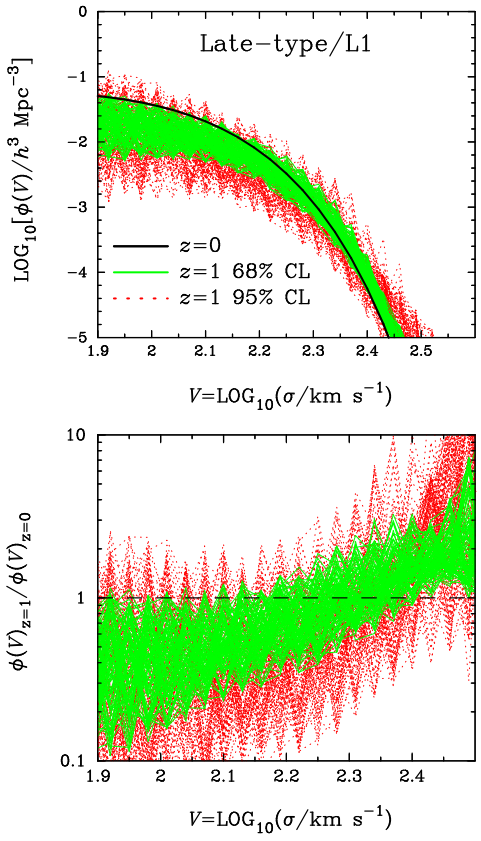

Figure 7. The same as Fig. 5 but for the late-type population of galaxies.

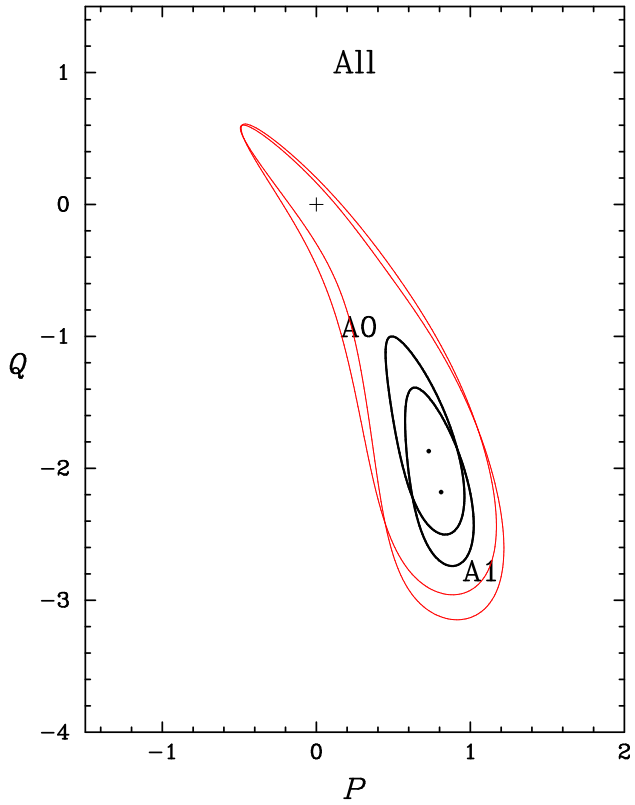

Figure 8. The same as Fig. 4 but for the total population of galaxies.

5.3 All galaxies

We study the evolution of all galaxies as a whole using the total VDFs A0 and A1 in Table 1. One advantage of constraining the evolution of the total VDF is that it is not affected by the uncertainties in the identification of the lensing galaxy type for several systems. However, parametric modelling of the total VDF is less straightforward because the total VDF has more parameters (equation 8) than the type-specific VDF (equation 2). Namely, there arise more severe degeneracies amongst the evolutions of the parameters. To break the parameter degeneracies we choose to fix the parameters of the correction term in equation (8), i.e. α' and ε. Fig. 8 shows the 68% and 95% CLs in the P-Q plane. The fitted parameter values can be found in Table 4. Notice that the fitted values of the evolution parameters are quite different from those of the early-type VDF because of the differences in the VDF functions as well as the data used.

In Fig. 9 the total VDFs at $z = 0$ are compared with the projected total VDFs at $z = 1$. The inferred evolutionary trends of the total VDFs are consistent with those of the type-specific VDFs. There are only relatively minor quantitative differences between the total VDF and the type-specific VDFs in the detailed nature of the evolution. Most noticeably, the number density evolution starts to become important at $\sigma \approx 200\,\mathrm{km\ s^{-1}}$ from the inferred evolution of the total VDF (whereas it starts at $\sigma \approx 250\,\mathrm{km\ s^{-1}}$ for the early-type VDF) and the degree of evolution for large velocity dispersion galaxies is greater for the total VDF than

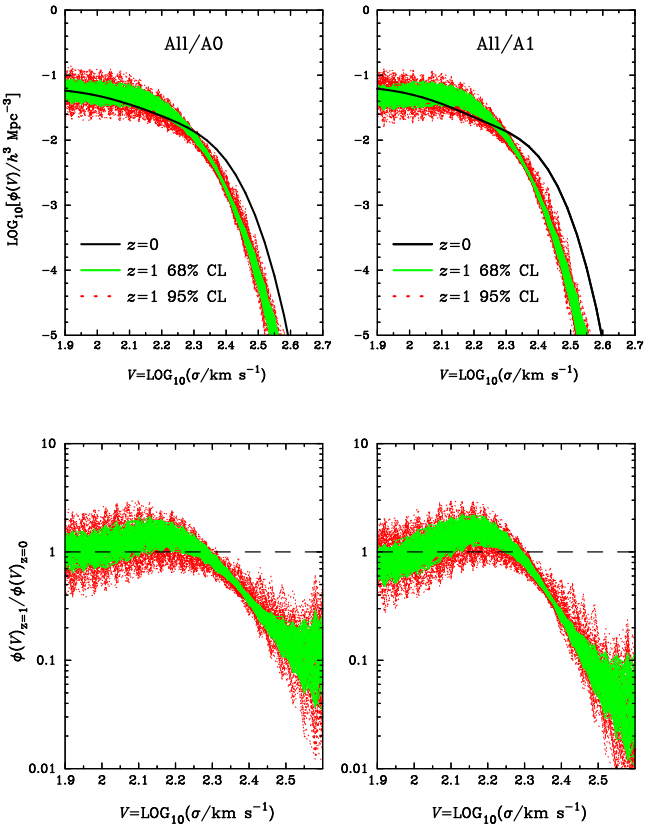

Figure 9. The same as Fig. 5 but for the total population of galaxies.

the early-type VDF. These minor quantitative differences are due to the differences both in the functional form of the VDF and the data used between the total VDF and the early-type VDF. The differences may reflect a possible range of errors. Despite the minor quantitative differences in the evolution between the total VDF and the early-type VDF, the overall trends of the evolution for large velocity dispersion galaxies are essentially the same.

6 DISCUSSION

6.1 Possible sources of systematic errors

6.1.1 (The interpretations of) the strong lensing data

The results presented in §5 are based on the most likely interpretation of the strong lensing data as judged by the author. However, the present data do not exclude alternative interpretations of the strong lensing systems. We assess here the greatest possible effects on galaxy evolution of alternative interpretations of the strong lensing data.

First, it is possible that the source redshift for B2045+265 is $z_s = 1.28$ and accordingly the velocity dispersion of the lensing galaxy is $\sigma \approx 384\,\mathrm{km\ s^{-1}}$. We judge that this interpretation is unlikely based on the following arguments. First of all, the measured velocity dispersion of the lensing galaxy as reported by Hamana et al. (2005) is $\sigma = 213 \pm 23\,\mathrm{km\ s^{-1}}$ which is much lower than the implied SIS velocity dispersion. If the measurement is correct and the source redshift is $z_s = 1.28$, this system would be an extremely rare case in which the SIS velocity dispersion is much larger than the measured stellar velocity dispersion ($\sigma_{\rm stars}/\sigma_{\rm SIS} = 0.55 \pm 0.06$). For the Sloan Lens ACS Survey (SLACS) sample of 53 early-type lens galaxies with $170\,\mathrm{km\ s^{-1}} < \sigma_{\rm stars} < 400\,\mathrm{km\ s^{-1}}$ Bolton et al. (2008) find $0.7 < \sigma_{\rm stars}/\sigma_{\rm SIS} < 1.3$ with a mean value close to unity. Secondly, according to Hamana et al. (2005) the lensing galaxy in B2045+265 lies in the fundamental plane with the measured velocity dispersion implying that it is a normal elliptical galaxy with the 'correct' velocity dispersion. Thirdly, the source redshift $z_s = 1.28$ for B2045+265 would give a much worse χ^2 for the model fit ($\Delta\chi^2 > 12$ for the evolution model of the total VDF). This means that the source redshift $z_s = 1.28$ for B2045+265 is not in harmony with all the other lens systems. Finally, the suggestion of $z_s = 1.28$ is based only on a single broad emission line (Fassnacht et al. 1999). This is far from a secure redshift from the observational point of view alone. Nevertheless, if we consider $z_s = 1.28$ and so take $\sigma = 384\,\mathrm{km\ s^{-1}}$ ignoring the Hamana et al. (2005) measurement of $\sigma = 213 \pm 23\,\mathrm{km\ s^{-1}}$ for B2045+265, the evolutions of the early-type VDF and the total VDF would change significantly at the high end of velocity dispersion. In Fig. 10 the total VDF A0 at $z = 0$ is compared with its projected VDF at $z = 1$ with $z_s = 1.28$ for B2045+265. The ratio $\phi_{z=1}/\phi_{z=0}$ decreases up to $\sigma \sim 300\,\mathrm{km\ s^{-1}}$ but then turns upward so that it approaches near unity within the 68% CL (although it is not shown) as σ reaches $400\,\mathrm{km\ s^{-1}}$. Namely, in this model the most massive early-type galaxies are already in place at $z = 1$ and there is little change in their number density since then. Overall the number density of early-type galaxies as a function of velocity dispersion is consistent with no evolution at 95% confidence between $z = 1$ and $z = 0$. This is in stark contrast to the results presented in §5 without $z_s = 1.28$ for B2045+265 that require the greater evolution at the larger velocity dispersion for $\sigma \gtrsim 200\,\mathrm{km\ s^{-1}}$. Given this potentially large systematic error, it is important to measure more reliably the source redshift and confirm the stellar velocity dispersion of Hamana et al. (2005) for B2045+265.

Second, the environments of the lensing galaxies may cause biases in inferring the velocity dispersions of the lensing galaxies from the observed image separations. We corrected the effects of the secondary (and tertiary) lensing galaxies within the image regions based on the results of detailed lens modelling found in the literature (Table 3). However, we ignored the possible effects of groups or clusters surrounding (and galaxies nearby) the image regions. It is thus possible that the velocity dispersions of the lensing galaxies were overestimated for some fraction of the lenses. There have been no systematic observations on the environments of the CLASS or the Snapshot lenses. However, a recent study of the environments of the SLACS lenses finds that typical contributions from the environments of the 'normal' lenses (i.e. those without very close companions) are less than a few per cent in the lensing mass density (Treu et al. 2008). For other several lens systems (including some CLASS and Snapshot lenses) with identified surrounding groups/clusters recent studies find that the environments contribute typically less than 10% to the convergence of the lens potential (Momcheva et al. 2006; Auger et al. 2007; Fassnacht et al. 2008). Since the lens surface density is pro-

portional to the velocity dispersion squared, neglection of the environmental contributions would cause errors in the velocity dispersion at most about 3%. Theoretical simulations by Keeton & Zabludoff (2004) predict somewhat larger error of 6% for the velocity dispersion. To assess a maximum possible systematic error arsing from neglecting the lens environments we consider lowering the observed image separation by 25% for the nine lens systems with a group (or groups) along the sight line (see table 2) assuming that the implied velocity dispersion is biased by 5%. The evolution of the total VDF A0 for this case can be found in Fig. 10. The best-fit for this case gives a better χ^2 ($\Delta\chi^2 = -2.5$) compared with the case that the surrounding groups contribute nothing to the image separations. However, the evolutionary behaviour of the VDF is little changed.

6.1.2 Statistical properties of sources

For the statistical analysis of strong lensing the properties of the source population are of crucial importance. The statistical properties of the source population influence the lensing probabilities through its redshift distribution and number-magnitude (or number-flux density) relation or through an evolving luminosity function collectively. Consequently, any error in the source properties can bias the results based on strong lensing statistics. For the present work, we use two distinct populations of sources, namely optical quasars and flat-spectrum radio sources (CLASS sources). For the optical quasar population the source redshifts are all known and the number-magnitude relation is also known empirically. For the flat-spectrum radio source population the source properties are less certain. For most of the radio sources the redshifts are not known and the inferred redshift distribution for the source population was largely based on 27 measured redshifts for a subsample of sources with 5 GHz flux densities between 25 mJy and 50 mJy (Marlow et al. 2000). Since lensed sources can come from flux densities below 25 mJy, it has been assumed for the previous analyses of the CLASS lensing that the redshift distribution is unchanged for sources below 25 mJy. Hence it is possible that the present work suffers from a systematic error in the CLASS parent source redshift distribution. However, McKean et al. (2007a) reports (a preliminary result) that the mean redshift for a sample of flat-spectrum sources with 5 GHz flux densities between 5 mJy and 15 mJy is consistent with that for sources of higher flux densities by Marlow et al. (2000). The number-flux density relation of the flat-spectrum radio sources is well measured above 30 mJy at 5 GHz because it is based on a large number ($\sim 10^4$) of source counts. It is less certain below 30 mJy because such a large number of sources are not available. Nevertheless, McKean et al. (2007a) gives a measurement of the number-flux density relation below 30 mJy based on a sample of 117 sources down to 5 mJy and confirms a previous estimate reported by Chae et al. (2002).

As discussed above there is no observational indication that the source properties adopted in this work are grossly biased. However, the uncertainties in the CLASS source properties clearly require further observational studies. It is thus of interest to see whether the two independent statistical lens samples, namely the Snapshot sample and the CLASS statistical sample, give agreeing results. The

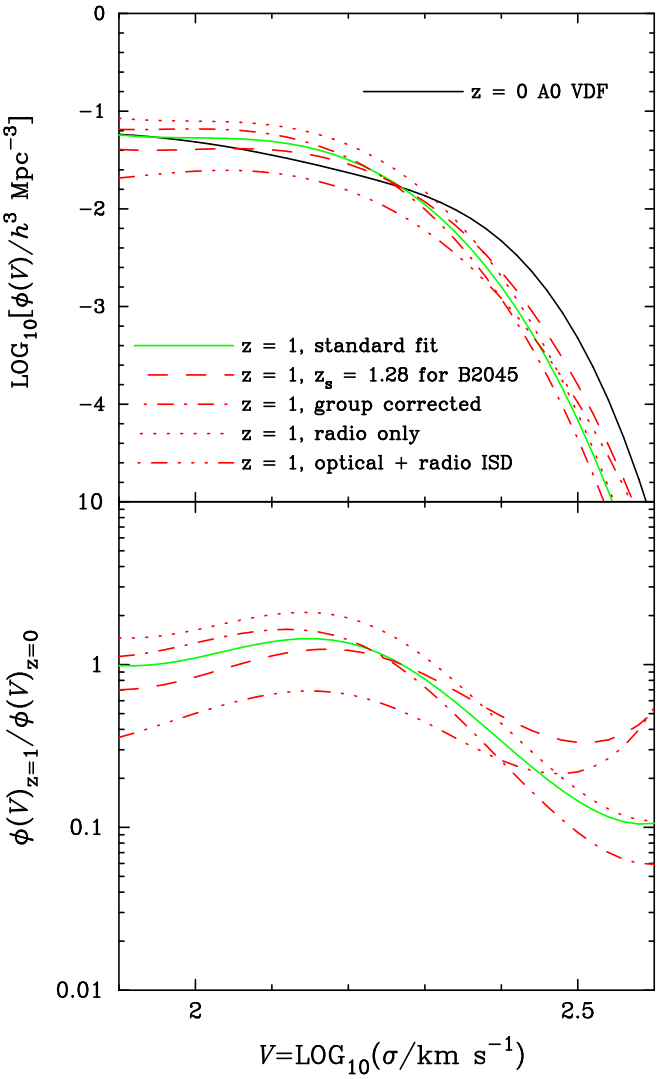

Figure 10. Possible systematic errors in the evolution of the VDF. The green solid line is the best-fit for the A0 VDF as shown in Fig. 9. The red dashed line is the fit assuming that the source redshift $z_s = 1.28$ is adopted *and* interpreted to give $\sigma \approx 384\,\mathrm{km\ s^{-1}}$ for the lensing galaxy in B2045+265. The red dash-dot line is the fit assuming that the surrounding groups contributed significantly to the image separations and the cross sections for several systems (see the texts in §6.1.1). The red dotted and dash-dot-dot-dot lines are the fits respectively including only the CLASS sample and only the Snapshot sample for the absolute lensing probability.

two independent results can provide a cross check of each other. Unfortunately, the Snapshot sample contains only four lenses so that it has a weak statistical power in constraining the evolution of the VDF. In particular, the Snapshot data alone cannot constrain the shape of the VDF at all. We thus include the image separation distribution (ISD) of all 26 radio lenses for the Snapshot fit. Notice that the ISD of the radio lenses does not depend on the statistical properties of the CLASS parent source population so that the inclusion of the radio ISD does not bias the result of the Snapshot fit. In Fig. 10 the radio and the Snapshot best-fit results are compared. Although not shown in the figure the 68% CLs of the two results overlap so that they are consis-

tent with each other. However, the best-fit results indicate that the Snapshot sample requires more evolution overall but less evolution at the high mass end than the CLASS sample.

6.1.3 Galaxy mass profiles

The results of this work are based on the assumption that the galactic mass distribution follows the isothermal distribution in the inner region of the galaxy probed by strong lensing (within about the effective radius). This assumption naturally leads to the equality of the observed stellar velocity dispersion and the SIE model velocity dispersion. Conversely, if the SIE assumption is systematically violated the lens statistics cannot reliably constrain the observed local stellar velocity dispersion. Of course, not all galaxies will closely follow the isothermal mass profile. However, the deviations of individual galaxies from the isothermality would not matter much statistically as long as the average profile is close to the isothermal.

Systematic errors from the isothermality assumption can arise in the following two contexts. First, if the mass profile varies systematically depending on the velocity dispersion, e.g. a higher velocity dispersion galaxy follows a shallower profile on average (or vice versa), then the results of this work can be systematically biased. The solution to this potential problem appears to be provided in part by the SLACS study of early-type galaxies through a combination of lens modelling and stellar velocity dispersion measurement of lensing galaxies. Bolton et al. (2008) finds through an analysis of 53 massive early-type galaxies that the mass profiles of early-type galaxies scatter around the isothermal profile but the average profile is close to the isothermal profile independent of the velocity dispersion between $175\,\mathrm{km\ s^{-1}}$ and $400\,\mathrm{km\ s^{-1}}$. The Bolton et al. (2008) finding applies to the upper velocity dispersion part to the peak velocity dispersion ($\sim 160\,\mathrm{km\ s^{-1}}$) of the early-type VDF. For the early-type galaxies of the peak velocity dispersion and lower, it remains unanswered whether the isothermality assumption is systematically unbiased. However, down to the velocity dispersion limit ($\sigma \approx 95\,\mathrm{km\ s^{-1}}$) sensitive to the strong lensing data (remember that this study is limited by the image separation range) most early-type galaxies are likely to be normal elliptical/lenticular galaxies with little contamination of dwarf ellipticals/lenticulars (see, e.g., de Rijcke et al. 2005). Hence it is likely that the isothermality assumption remain not so bad for low velocity dispersion galaxies within the range probed by this work. For the late-type galaxies it is expected that the mass profile becomes systematically shallower in the inner region ($\lesssim R_{\rm d}$[5]) as the luminosity decreases for sub-L_* galaxies according to the rotation curves of spiral galaxies (Persic et al. 1996). However, for the range of galaxies probed by the strong lensing data (circular rotation speed $V_c \gtrsim 134\,\mathrm{km\ s^{-1}}$) the deviations are not likely to be too large. The effects of the neglected errors can be understood as follows. The assumed constant rotation curve for a galaxy whose rotation speed actually declines toward the galactic centre will inflate the lensing mass and so the lensing cross section. This inflated lensing cross section will then lead an underestimate of the number density so as to keep the observed lensing occurrences. Consequently, the evolution of the number density for the late-type population can be overestimated. We postpone the quantification of this systematic error to a future work although it may not be warranted because of the small number statistics of late-type lenses in the present data.

Second, if the average mass profile of galaxies deviates systematically from the isothermal as z increases, then the results on the galaxy number density evolution from this work can be biased. The total (luminous plus dark) mass profiles of galaxies at intermediate and higher redshifts can be best constrained by modelling strong lens systems provided with reliable and stringent observational constraints. The best studied examples in strong lensing appear to suggest that the average total mass profile of galaxies is isothermal up to $z \sim 1$.[6] Koopmans et al. (2006) carry out a systematic modelling of SLACS lenses and find that the mass profiles of gravitational lens galaxies are close to isothermal regardless of the lens redshifts between $z = 1$ and $z = 0$. The Koopmans et al. (2006) sample contains 6 lenses for $0.5 \lesssim z \lesssim 1$, so that the isothermality may be valid at least up to $z \sim 0.7$. Individual extensive modelling of lenses at $z \sim 1$ also find isothermal(-like) total mass distributions of galaxies. Saha et al. (2007) find a nearly isothermal profile from a non-parametric modelling of MG0414+054 at $z = 0.96$. Winn et al. (2004) model J1632-0033 at $z \sim 1$ and find a tight constraint of $\beta = 1.91 \pm 0.02$ for a mass density of $\rho(r) \propto r^{-\beta}$ ($\beta = 2$ corresponding to the isothermal) using an observed central image. Treu & Koopmans (2002) combines galactic dynamics and lens modelling to find $\beta = 2.0 \pm 0.1(\mathrm{stat}) \pm 0.1(\mathrm{syst})$ for MG 2016+112 at $z = 1.004$. Moreover, there exist many modelling examples in which the authors assume the isothermal profile for the lensing galaxies at $z \sim 1$ and reproduce the observed image properties although some systems appear to require substructures. To sum up, strong lensing studies support the isothermal profile up to $z \sim 1$ without any indication of evolution of the total mass profile in redshift. The total mass profiles can also be constrained by other dynamical probes although few studies have been carried out at $z \gtrsim 1$. van der Wel & van der Marel (2008) present velocity dispersion profiles of early-type galaxies up to ~ 4 kpc ($0''.5$) at $z \sim 1$ which are consistent with isothermal profiles.

Studies based on surface photometry find varying results on the evolution of the galaxy mass profiles. Many recent studies suggest that high redshift ($z \gtrsim 1$) galaxies may be more compact in their light and stellar mass density distributions than the local counterparts (e.g. Trujillo et al. 2007; van der Wel et al. 2008; Cimatti et al. 2008; van Dokkum et al. 2008; Bezanson et al. 2009). In particular, Bezanson et al. (2009) find that the stellar mass density profiles at $z \sim 2.3$ are more steeply declining beyond $r = 1$ kpc than the local counterparts. Bezanson et al. (2009) also note that the stellar density within 1 kpc is 2-3 times higher at $z \sim 2.3$ than at $z \sim 0$. This structural evo-

[5] The disk scale length in the exponential disk.

[6] It is now well established that lensing galaxies at intermediate redshifts $z \sim 0.3 - 0.7$ have isothermal (or close to isothermal) mass profiles. The question here is whether the isothermality would hold up to $z = 1$.

lution may be explained by galaxy evolution through minor mergers (Naab et al. 2009, 2007). On the other hand, Hopkins et al. (2009) find similar densities for the observed physical radius range both at $z > 2$ and at $z \sim 0$. Hopkins et al. (2009) further note that there may or may not be differences in the densities outside the central regions between $z > 2$ and $z \sim 0$. The ambiguity outside the central regions arises primarily from the difficulty in observing the low surface brightness parts. Interestingly, Saracco et al. (2009) find that early-type galaxies at $1 < z < 2$ may be divided into two groups, one group showing no size evolution and the other group implying a significant size evolution compared with local galaxies. These studies may imply that at least some galaxies undergo size evolutions possibly including stellar mass profile evolutions. Complicating the issue, dark mass profiles may also evolve as a result of (responding to) stellar mass growth and dark mass growth via merging. Unfortunately, the baryon-involved evolution of dark mass profile is a poorly understood part of galaxy evolution. Consequently, the surface photometry data alone cannot settle the issue of the total mass profile evolution even if the stellar mass profile evolution is real.

As described above direct probes of the galaxy mass profiles give support for the isothermality up to $z = 1$. However, the evidence is not broad and strong enough to rule out the variation from the isothermality in z and/or σ (or mass). Hence galaxy mass profiles remain a source of uncertainty. If the true mass profiles deviate systematically as a function of z and/or σ, then the number density evolution in z as a function of σ will be biased. Namely, the variation in mass profile leads to the variation in the cross section and the magnification bias resulting in a different number density evolution. Roughly speaking, if the true mass profile is steeper/more concentrated (shallower/less concentrated) at $z = 1$ than the isothermal profile, then the number density at $z = 1$ should be lower (higher) than that derived here based on the isothermal profile. It is unclear at present how important the effects turn out to be quantitatively. A realistic ray-tracing simulation would eventually be required to quantify the effects robustly.

6.1.4 Local velocity dispersion functions

The local velocity dispersion function provides a benchmark for the study of galaxy evolution just as the local luminosity function is. Hence we cannot overemphasise the importance of reliable local VDFs for this work. For this reason we have considered not only the measured early-type VDF by Choi et al. (2007) but also the Monte Carlo simulated VDFs for both the early-type and the late-type populations based on the galaxy counts from the SDSS and the intrinsic correlations between luminosity and internal velocities.

Despite the range of the VDFs considered in this work one may still consider the following systematic errors for the local VDFs. First of all, the galaxy counts for the type-specific galaxy populations remain somewhat uncertain due to the error in the galaxy classifications. The Choi et al. (2007) classification matches relatively well the morphological classification. However, even the Choi et al. (2007) classification has an error of about 10% according to Park & Choi (2005).

Second, the early-type VDF is less reliable at lower velocity dispersions ($\sigma \lesssim 150\,\mathrm{km\ s^{-1}}$) because of the incompleteness in the volume and magnitude limited samples of galaxies used by Choi et al. (2007) to obtain the early-type VDF and the intrinsic correlation between luminosity and velocity dispersion. Indeed, a Monte Carlo simulated SDSS galaxy sample makes a difference in the early-type VDF at velocity dispersions $\lesssim 125\,\mathrm{km\ s^{-1}}$ (see Fig. 2). However, the present strong lensing data are sensitive only to velocity dispersions $\gtrsim 95\,\mathrm{km\ s^{-1}}$ so that the difference in the VDF for $\sigma \lesssim 125\,\mathrm{km\ s^{-1}}$ makes little difference in the results on the evolution of the VDF.

Finally, the late-type VDF is relatively less reliable. We turned the circular rotation speed to the velocity dispersion assuming the SIS profile for all late-type galaxies, but the observed mass profile deviates systematically from the isothermal toward the galactic centre. In this respect the late-type VDF may not be well-defined and it may be eventually necessary to use directly the circular velocity function for the statistics of strong lensing through a realistic lens model of a late-type (spiral) galaxy. Such a realistic modelling will become very important in the future when the number statistics of late-type lenses becomes large.

6.2 Comparison with previous results in lensing statistics

The importance of galaxy evolution in strong lensing statistics was recognised and applied to a handful of lenses for the first time by Mao (1991) and Mao & Kochanek (1994). However, strong lensing statistics has usually been used to constrain the cosmological constant (and dark energy) and appears to confirm the concordance cosmology according to recent results assuming the early-type population evolves little between $z = 1$ and now (e.g. Chae et al. 2002; Mitchell et al. 2005; Chae 2007; Oguri et al. 2008). The assumption of no-evolution of the early-type population appeared also to be supported by strong lensing statistics assuming the concordance cosmological model according to an analysis of the CLASS statistical sample by Chae & Mao (2003) and a lens-redshift test by Ofek et al. (2003). Notice that these studies assumed a constant shape of the the inferred velocity dispersion function. In other words, Chae & Mao (2003) and Ofek et al. (2003) considered only the evolution of the number density and the characteristic velocity dispersion. More recently, Capelo & Natarajan (2007) carried out the lens-redshift test more extensively and studied in particular possible systematic errors based on a sample of 70 galaxy lenses. However, Capelo & Natarajan (2007) also assumed non-evolving shape for the VDF and obtained results consistent with earlier results. To sum up, all previous results on galaxy evolution from strong lensing statistics were based on the assumption of the non-evolving shape for the VDF and appeared to be consistent with no evolution of early-type galaxies.

In this work we allow the shape of the VDF to evolve and find that strong lensing statistics actually requires a differential evolution of the VDF (see Figs. 5 and 9). The differential evolution is intriguing in that the number density of galaxies changes little between $z = 1$ and now below $\sigma \approx 200\,\mathrm{km\ s^{-1}}$ but at higher velocity dispersions the number density evolution becomes significant with an increasingly larger factor for a higher velocity dispersion (see

Fig. 9). We discuss the implications of this differential evolution below in §6.4. Here we just point out that this behaviour of differential evolution may explain why previous lens statistics resulted in little evolution assuming a constant shape. For a constant shape of the VDF its evolution may be realised only through the vertical and horizontal shifts, namely the variations of the integrated number density and the characteristic velocity dispersion. The shifts of the VDF are likely to be determined by the behaviour of the number density at the lensing peak velocity dispersion, i.e. the velocity dispersion for which the lensing probability ($\propto \phi\sigma^4$) is maximal. However, as shown in Fig. 9 the number density of galaxies evolves little at intermediate velocity dispersions. Consequently, the VDF appeared to evolve little by previous lensing statistics.

6.3 Comparison with theoretical predictions and galaxy surveys: a qualitative analysis

In the ΛCDM hierarchical structure formation picture the dark halo mass function (DMF) evolves in cosmic time as a consequence of hierarchical merging (e.g. White & Rees 1978; Lacey & Cole 1993). Accordingly, the stellar mass function (SMF) and the velocity dispersion function (VDF) of galaxies also evolve. However, baryon physics complicates the evolutions of the SMF and the VDF making it non-trivial to compare the evolutions of the DMF, the SMF and the VDF one another. Conversely, careful analyses of the coevolution of the DMF, the SMF and the VDF may reveal key insights into galaxy formation and evolution processes (Chae 2010). Here we compare the evolutionary trends of the VDF from this work against the DMF from N-body simulations and the SMFs predicted by recent semi-analytical models of galaxy formation and obtained by cosmological surveys of galaxies. This is meant to be an inter-comparison of the *qualitative* features of three functions as suggested by current theoretical and observational studies. A comprehensive and quantitative analysis of the coevolution of three functions is given in Chae (2010) where evolutions of functions $\sigma(M_{\rm vir})$ and $\sigma(M_{\rm stars})$ are derived and their implications are discussed in the context of current cosmological observations.

A generic prediction of the ΛCDM theory is the differential evolution of the DMF in which the number density evolution of a larger $M_{\rm vir}$ (virial mass) halo is greater, e.g. since $z = 1$ (see Fig. 11). As can be noticed easily, this evolutionary trend is strikingly similar to that of the total VDF (Fig. 9). In fact, this *qualitative* similarity is expected once we assume that σ is on average a monotonically increasing function of $M_{\rm vir}$ at each epoch (a plausible assumption). The quantitative detail of the evolution of $\sigma(M_{\rm vir})$ has implications on the structural evolution of the galaxy-halo system (Chae 2010).

Unlike the DMF the evolution of the SMF is not well predicted by theoretical models because of complex galaxy formation processes. Nevertheless, it appears that recent semi-analytic models (SAMs) predict a hierarchical evolution of the SMF that shows evolutionary patterns similar to those of the DMF and the SMF (see Fig. 12). However, the 'observed' SMFs from galaxy surveys show different evolutionary patterns (Fig. 12). In particular, many galaxy surveys suggest stellar mass-downsizing (apparently anti-

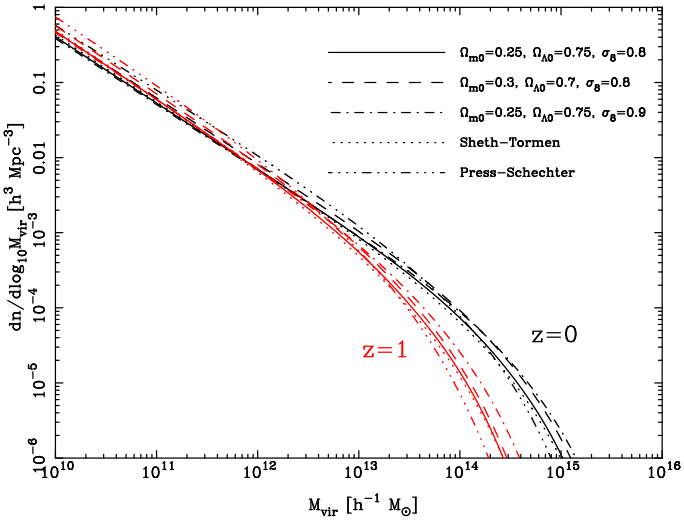

Figure 11. The evolution of the dark halo mass function (DMF) between $z = 0$ and $z = 1$ under the current ΛCDM paradigm. The results are based on the code provided by Reed et al. (2007). Notice that the DMF evolution is differential for $M_{\rm vir} \gtrsim 10^{13} h^{-1}{\rm M}_\odot$ as is the VDF evolution for $\sigma \gtrsim 200\,{\rm km\ s^{-1}}$ (see Fig. 9).

hierarchical) evolution of galaxies (e.g., Cimatti et al. 2006; Fontana et al. 2006; Pozzetti et al. 2007; Conselice et al. 2007; Scarlata et al. 2007; Cool et al. 2008; Marchesini et al. 2009), although there are results that do not particularly support stellar mass-downsizing (e.g., Bell et al. 2004; Faber et al. 2007; Brown et al. 2008; Ilbert et al. 2009). The disagreement between SAM predictions and galaxy survey results is more apparent for lower stellar mass galaxies. Some authors (e.g. Fontanot et al. 2009) suggest that this disagreement reflects some additional physical processes missing in the current SAMs. However, assuming that σ is on average a monotonically increasing function of $M_{\rm stars}$ at each epoch, we may expect a hierarchical evolution of the SMF. In this view, the VDF evolution is *qualitatively* more in line with the current SAM predictions than the downsizing SMFs from galaxy surveys. However, if downsizing SMFs from galaxy surveys should turn out to be true, a deeper rethinking of $\sigma(M_{\rm stars})$ may be required. A detailed quantitative analysis of the evolution of $\sigma(M_{\rm vir})$ based on currently available data is carried out in Chae (2010).

7 SUMMARY AND CONCLUSIONS

In this work we have constrained the evolutionary behaviours of the velocity dispersion functions of galaxies based on the local measured and Monte Carlo realised VDFs and the statistics of strongly-lensed radio-selected and optically-selected sources. This work is also based on the assumption that the total (luminous plus dark) mass profile is isothermal in the optical region for $0 \leqslant z \leqslant 1$ in line with strong lens modelling results. The constrained evolutions of the VDFs can be characterised as follows.

- The (comoving) number density of massive galaxies with $\sigma \gtrsim 200\,{\rm km\ s^{-1}}$, which are mostly early-type galaxies, evolves differentially from $z = 1$ to $z = 0$ in the way that

the evolution is greater at a higher velocity dispersion. The most massive galaxies of $\sigma \sim 400\,\mathrm{km\ s^{-1}}$ are much rarer at $z = 1$ than the present epoch with its number density probably less than 30% of the local density.

• The number density of intermediate-mass galaxies with $95\,\mathrm{km\ s^{-1}} \lesssim \sigma \lesssim 200\,\mathrm{km\ s^{-1}}$ are nearly constant between $z = 1$ and $z = 0$ regardless of the morphological type.

• The velocity dispersion function of late-type galaxies transformed from the Monte Carlo realised circular velocity function is consistent with no evolution between $z = 1$ and $z = 0$ either in the overall number density or its shape.

Comparing the constrained VDFs with the ΛCDM DMF and the SMFs observed from galaxy surveys as well as predicted from semi-analytical models of galaxy formation, we find the following.

• The VDF evolution is in line with the evolution of the ΛCDM DMF, i.e., the hierarchical build-up of mass structures over cosmic time.

• The evolutionary pattern of the VDF is similar to the SMF evolution predicted by recent semi-analytical models of galaxy formation but qualitatively different from the stellar mass-downsizing evolution suggested by galaxy surveys. Further investigations are required to clarify this apparent conflict.

In conclusion we have investigated in detail the evolutionary behaviours of the VDFs for the first time based on local SDSS data and statistical strong lensing data and found that the evolution pattern is strikingly similar to that of the ΛCDM DMF. Also, there is a promising agreement between the VDF evolution and the SMF evolution predicted by SAMs although observed stellar mass-downsizing evolution needs yet to be clarified. Larger well-defined statistical samples of strong lensing from future observation tools like the SKA will be invaluable laboratories for decoding galaxy formation and evolution processes.

This work makes use of a number of hard-worked observational results from cosmological surveys including but not limited to the CLASS, the PANELS, the HST Snapshot, the SDSS and the 2dF. The author thanks the anonymous referee for insightful comments and useful suggestions for presentations. The author received useful comments on the originally submitted version of this manuscript from Michael Brown, Lawrence Tresse and Ignacio Trujillo. The author would like to thank Changbom Park and Myungshin Im for useful discussions. The author also would like to thank Shude Mao for comments on the manuscript.

REFERENCES

Almeida C., Baugh C. M., Wake D. A., Lacey C. G., Benson A. J., Bower R. G., Pimbblet K., 2008, MNRAS, 386, 2145
Auger M. W., Fassnacht C. D., Abrahamse A. L., Lubin L. M., Squires G. K., 2007, AJ, 134, 668
Bell E. F., McIntosh D. H., Katz N., Weinberg M. D., 2003, ApJS, 149, 289
Bell E. F., et al., 2004, ApJ, 608, 752
Bezanson R., van Dokkum P. G., Tal T., Marchesini D., Kriek M., Franx M., Coppi P., 2009, ApJ, 697, 1290
Biggs A. D., et al., 2003, MNRAS, 338, 1084
Blanton M. R., et al., 2003, ApJ, 592, 819
Bolton A. S., Treu T., Koopmans L. V. E., Gavazzi R., Moustakas L. A., Burles S., Schlegel D. J., Wayth R., 2008, ApJ, 684, 248
Borch A., et al., 2006, A&A, 453, 869
Bower R. G., Benson A. J., Malbon R., Helly J. C., Frenk C. S., Baugh C. M., Cole S., Lacey C. G., 2006, MNRAS, 370, 645
Brown M., et al., 2007, ApJ, 654, 858
Brown M. J. I., Zheng Z., White M., Dey A., Jannuzi B. T., Benson A. J., Brand K., Brodwin M., Croton D. J., 2008, ApJ, 682, 937
Browne I. W. A. et al., 2003, MNRAS, 341, 13
Bundy K., et al., 2006, ApJ, 651, 120
Capelo P. R., Natarajan P., 2007, NJPh, 9, 445
Cappellari M., et al., 2006, MNRAS, 366, 1126
Cattaneo A., Dekel A., Faber S. M., Guiderdoni B., 2008, MNRAS, 389, 567
Chae K.-H., 2003, MNRAS, 346, 746
Chae K.-H., 2005, ApJ, 630, 764
Chae K.-H., 2007, ApJ, 658L, 71
Chae K.-H., 2010, MNRAS, to be submitted
Chae K.-H. et al., 2002, Phys. Rev. Lett., 89, 151301
Chae K.-H., Mao S., 2003, ApJ, 599, L61
Chae K.-H., Mao S., Augusto P., 2001, MNRAS, 326, 1015
Choi, Y.-Y., Park, C., & Vogeley, M. S. 2007, ApJ, 658, 884
Cimatti A., Daddi E., Renzini A., 2006, A&A, 453, L29
Cimatti A., et al., 2008, A&A, 482, 21
Cohn J. D., Kochanek C. S., McLeod B. A., Keeton C. R., 2001, ApJ, 554, 1216
Cole S., et al., 2001, MNRAS, 326, 255
Congdon A. B., Keeton C. R., 2005, MNRAS, 364, 1459
Conroy C., Wechsler R. H., 2009, ApJ, 696, 620
Conselice C. J., et al., 2007, MNRAS, 381, 962
Cool R. J., et al., ApJ, in press (arXiv:0804.4516)
Croton D. J., et al., 2005, MNRAS, 356, 1155
Croton D. J., Springel V., White S. D. M., de Lucia G., Frenk C. S., Gao L., Jenkins A., Kauffmann G., Navarro J. F., Yoshida N., 2006, MNRAS, 365, 11
de Lucia G., Springel V., White S. D. M., Croton D., Kauffmann G., 2006, MNRAS, 366, 499
de Rijcke S., Michielsen D., Dejonghe H., Zeilinger W. W., Hau G. K. T., 2005, A&A, 438, 491
Dunkley J., et al., 2009, ApJS, 180, 306
Drory N., Bender R., Feulner G., Hopp U., Maraston C., Snigula J., Hill G. J., 2004, ApJ, 608, 742
Faber S. M., Jackson R. E., 1976, ApJ, 204, 668
Faber S. M., et al., 2007, ApJ, 665, 265
Fassnacht C. D. et al., 1999, AJ, 117, 658
Fassnacht C. D., Kocevski D. D., Auger M. W., Lubin L. M., Neureuther J. L., Jeltema T. E., Mulchaey J. S., McKean J. P., 2008, ApJ, 681, 1017
Fontana A., et al., 2006, A&A, 459, 745
Fontanot F., De Lucia G., Monaco P., Somerville R. S., Santini P., 2009, MNRAS, 397, 1776
Gavazzi R., et al., 2007, ApJ, 667, 176
Gonzalez A. H., Williams K. A., Bullock J. S., Kolatt T. S., Primack J. R., 2000, ApJ, 528, 145

Hamana T., Ohyama Y., Chiba M., Kashikawa N., 2005, astro-ph/0507056
Hopkins P. F., Bundy K., Murray N., Quataert E., Lauer T. R., Ma C.-P., 2009, MNRAS, in press (arXiv: 0903.2479)
Ilbert O., et al., 2006, A&A, 453, 809
Ilbert O., et al., 2009, arXiv:0903.0102
Inada N., et al., 2008, AJ, 135, 496
Jing Y. P., Suto Y., 2002, ApJ, 574, 538
Keeton C. R., Zabludoff A. I., 2004, ApJ, 612, 660
Keeton C. R., Winn J. N., 2003, ApJ, 590, 39
King L. J., Browne I. W. A., Muxlow T. W. B., Narasimha D., Patnaik A. R., Porcas R. W., Wilkinson P. N., 1997, MNRAS, 289, 450
Kitzbichler M. G., White S. D. M., 2007, MNRAS, 376, 2
Kochanek C. S., 1996, ApJ, 466, 638
Kochanek C. S., et al., 2001, ApJ, 560, 566
Kochanek C. S., White M., 2001, ApJ, 559, 531
Koopmans L. V. E., Treu T., Bolton A. S., Burles S., Moustakas L. A., 2006, ApJ, 649, 599
Koopmans L. V. E., Treu T., Fassnacht C. D., Blandford R. D., Surpi G., 2003, ApJ, 599, 70
Lacey C, Cole S., 1993, MNRAS, 262, 627
Lehár J., Falco E. E., Kochanek C. S., McLeod B. A., Muñoz J. A., Impey C. D., Rix H.-W., Keeton C. R., Peng C. Y., 2000, ApJ, 536, 584
Lotz J. M., et al., 2008, ApJ, 672, 177
Mao S., 1991, ApJ, 380, 9
Mao S., Kochanek C. S., 1994, MNRAS, 268, 569
Maoz D., et al., 1993, ApJ, 409, 28
Maoz D., Rix H.-W., 1993, ApJ, 416, 425
Marchesini D., van Dokkum P. G., Förster S., Natascha M., Franx M., Labbé I., Wuyts S., 2009, ApJ, 701, 1765
Marlow D. R., Rusin D., Jackson N., Wilkinson P. N., Browne I. W. A., Koopmans L., 2000, AJ, 119, 2629
McKean J. P., Browne I. W. A., Jackson N. J., Fassnacht C. D., Helbig P., 2007a, MNRAS, 377, 430
McKean J. P., Koopmans L. V. E., Flack C. E., Fassnacht C. D., Thompson D., Matthews K., Blandford R. D., Readhead A. C. S., Soifer B. T., 2007b, MNRAS, 378, 109
Menci N., Fontana A., Giallongo E., Grazian A., Salimbeni S., 2006, ApJ, 647, 753
Mitchell J. L., Keeton C. R., Frieman J. A., Sheth R. K., 2005, ApJ, 622, 81
Momcheva I., Williams K., Keeton C., Zabludoff A., 2006, ApJ, 641, 169
Monaco P., Murante G., Borgani S., Fontanot F., 2006, ApJ, 652, 89
Moore B., Ghigna S., Governato F., Lake G., Quinn T., Stadel J., Tozzi P., 1999, ApJ, 524, 19
More A., McKean J. P., Muxlow T. W. B., Porcas R. W., Fassnacht C. D., Koopmans L. V. E., 2008, MNRAS, 384, 1701
Myers S. T. et al., 2003, MNRAS, 341, 1
Naab T., Johansson P. H., Ostriker J. P., 2009, ApJ, 699, 178
Naab T., Johansson P. H., Ostriker J. P., Efstathiou G., 2007, ApJ, 658, 710
Navarro J. F., Frenk C. S., White S. D. M., 1997, ApJ, 490, 493
Navarro J. F., Hayashi E., Power C., Jenkins A. R., Frenk C. S., White S. D. M., Springel V., Stadel J., Quinn T. R., 2004, MNRAS, 349, 1039
Norberg P., et al., 2002, MNRAS, 336, 907
Ofek E. O., Rix H.-W., Maoz D., 2003, MNRAS, 343, 639
Oguri M., et al., 2008, AJ, 135, 512O
Panter B., Jimenez R., Heavens A. F., Charlot S., 2007, MNRAS, 378, 1550
Park C., Choi Y.-Y., 2005, ApJ, 635, L29
Persic M., Salucci P., Stel F., 1996, MNRAS, 281, 27
Phillips P. M., et al., 2000, MNRAS, 319, 7
Pizagno J., Prada F., Weinberg D. H., Rix H.-W., Pogge R. W., Grebel E. K., Harbeck D., Blanton M., Brinkmann J., Gunn J. E., 2007, AJ, 134, 945
Pozzetti L., et al., 2007, A&A, 474, 443
Reed D. S., Bower R., Frenk C. S., Jenkins A., Theuns T., 2003, MNRAS, 346, 565
Rix H.-W., de Zeeuw P. T., Cretton N., van der Marel R. P., Carollo C. M., 1997, ApJ, 488, 702
Rubin V. C., Burstein D., Ford W. K. Jr., Thonnard N., 1985, ApJ, 289, 81
Rusin D., et al., 2001, ApJ, 557, 594
Rusin D., Kochanek C. S., 2005, ApJ, 623, 666
Saha P., Williams L. L. R., Ferreras I., 2007, ApJ, 663, 29
Salucci P., Lapi A., Tonini C., Gentile G., Yegorova I., Klein U., 2007, MNRAS, 378, 41
Saracco P., Longhetti M., Andreon S., 2009, MNRAS, 392, 718
Scarlata C., et al., 2007, ApJS, 172, 494
Sheth R. K. et al., 2003, ApJ, 594, 225
Siemiginowska A., Bechtold J., Aldcroft T. L., McLeod K. K., Keeton C. R., 1998, ApJ, 503, 118
Stringer M. J., Benson A. J., Bundy K., Ellis R. S., Quetin E. L., 2009, MNRAS, 393, 1127
Surpi G., Blandford R. D., 2003, ApJ, 584, 100
Treu T., Gavazzi R., Gorecki A., Marshall P. J., Koopmans L. V. E., Bolton A. S., Moustakas L. A., Burles S., 2008, ApJ, submitted (arXiv/0806.1056)
Treu T., Koopmans L. V. E., 2002, ApJ, 575, 87
Trujillo I., Conselice C. J., Bundy K., Cooper M. C., Eisenhardt P., Ellis R. S., 2007, MNRAS, 382, 109
Tully R. B., Fisher J. R., 1977, A&A, 54, 661
van der Wel A., Holden B. P., Zirm A. W., Franx M., Rettura A., Illingworth G. D., Ford H. C., 2008, ApJ, 688, 48
van der Wel A., van der Marel R. P., 2008, arXiv:0804.4228
van Dokkum P. G., et al., 2008, ApJ, 677L, 5
Winn J. N., Kochanek C. S., Keeton C. R., Lovell J. E. J., 2003, ApJ, 590, 26
Winn J. N., Hewitt J. N., Schechter P. L., 2001b, in Gravitational Lensing: Recent Progress and Future Goals, ASP Conference Proceedings, Vol. 237, ed. T. G. Brainerd & C. S. Kochanek (San Francisco: ASP), p. 61
Winn J. N., Rusin D., Kochanek C. S., 2004, Nature, 427, 613
White S. D. M., Rees M. J., 1978, MNRAS, 183, 341
York T., et al., 2005, MNRAS, 361, 259

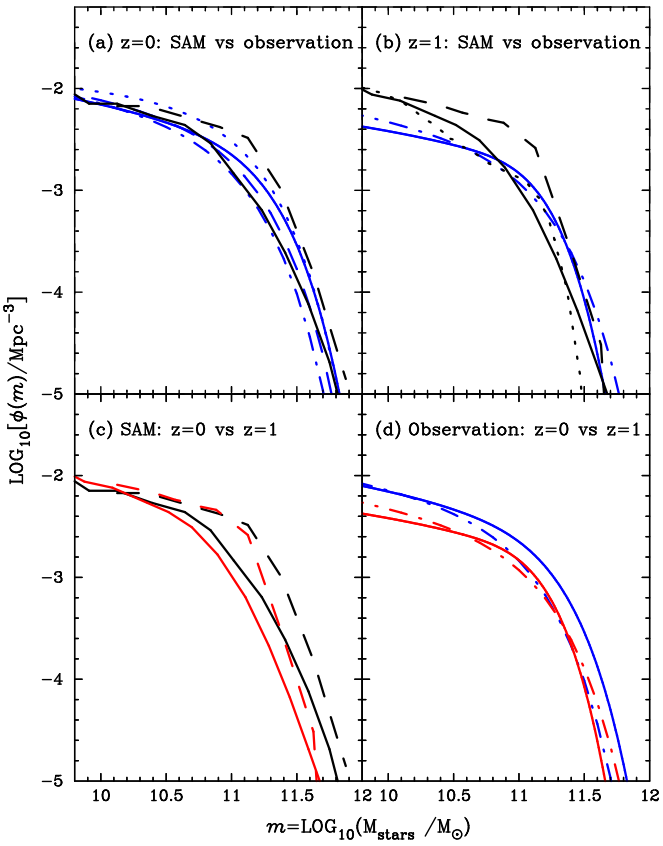

Figure 12. (a) Stellar mass functions (SMFs) of galaxies at $z = 0$. Blue solid, dashed, dash-dotted and dotted curves are respectively the observed SMFs from Ilbert et al. (2009), Panter et al. (2007), Conroy & Wechsler (2009) and Bell et al. (2003). Notice that the Conroy & Wechsler (2009) SMF is a composite of several galaxy survey results. Black solid curve is a median of the Fontanot et al. (2009) three semi-analytic model (SAM) predictions while black dashed curve is the prediction of the Cattaneo et al. (2008) SAM. (b) SMFs at $z = 1$. The colours and styles of the lines refer to the same references as in (a). Black dotted curve is the Stringer et al. (2009) SAM prediction. Notice the discrepancy between the observed SMFs and the predicted SMFs for the lower part of the stellar mass range. (c) SAM predicted SMFs at $z = 0$ and $z = 1$ are compared. Black curves refer to $z = 0$ while red curves refer to $z = 1$. Solid and dashed curves are respectively the predictions by Fontanot et al. (2009) and Cattaneo et al. (2008). Notice that these predicted SMFs show hierarchical differential evolutions in line with the VDF and the DMF (see Figs. 9 and 11). (d) Observed SMFs at $z = 0$ and $z = 1$ are compared. Blue curves refer to $z = 0$ while red curves refer to $z = 1$. Solid and dash-dotted curves are respectively the SMFs from Ilbert et al. (2009) and Conroy & Wechsler (2009). The composite SMF by Conroy & Wechsler (2009) shows an anti-hierarchical evolution while the COSMOS SMF by Ilbert et al. (2009) does not show such a differential evolution.